Fine-scale phytoplankton community transitions in the oligotrophic ocean: A Mediterranean Sea case study

Laurina Oms, Monique Messié, Jean-Christophe Poggiale, Gérald Grégori, Andrea Doglioli

▶ **To cite this version:**

Laurina Oms, Monique Messié, Jean-Christophe Poggiale, Gérald Grégori, Andrea Doglioli. Fine-scale phytoplankton community transitions in the oligotrophic ocean: A Mediterranean Sea case study. Journal of Marine Systems, 2024, 246, pp.104021. 10.1016/j.jmarsys.2024.104021 . hal-04799478

HAL Id: hal-04799478
https://hal.science/hal-04799478v1

Submitted on 23 Nov 2024

HAL is a multi-disciplinary open access archive for the deposit and dissemination of scientific research documents, whether they are published or not. The documents may come from teaching and research institutions in France or abroad, or from public or private research centers.

L'archive ouverte pluridisciplinaire **HAL**, est destinée au dépôt et à la diffusion de documents scientifiques de niveau recherche, publiés ou non, émanant des établissements d'enseignement et de recherche français ou étrangers, des laboratoires publics ou privés.

Distributed under a Creative Commons Attribution 4.0 International License

Journal of Marine Systems 246 (2024) 104021

Contents lists available at ScienceDirect

Journal of Marine Systems

journal homepage: www.elsevier.com/locate/jmarsys

Fine-scale phytoplankton community transitions in the oligotrophic ocean: A Mediterranean Sea case study

Laurina Oms [a,*], Monique Messié [b], Jean-Christophe Poggiale [a], Gérald Grégori [a], Andrea Doglioli [a]

[a] Aix Marseille Univ., Toulon University, CNRS, IRD, MIO UM 110, Marseille, 13288, France
[b] Monterey Bay Aquarium Research Institute, Moss Landing, CA, USA

ARTICLE INFO

Dataset link: https://github.com/OmsLaurina/toolbox_growthmodel

Keywords:
Trophic interactions
Fine-scales
Phytoplankton ecology
NPZ modelling
Cytometry

ABSTRACT

The vast diversity of marine phytoplankton, shaped by intricate water dynamics, remains poorly understood in the oligotrophic ocean. *In situ* studies reveal fine-scale dynamics affecting phytoplankton distribution, leading to abrupt shifts in abundance and biomass referred here as "phytoplankton community transitions" (PCTs). Using a simple nutrient–phytoplankton–zooplankton (NPZ) numerical model, our study proposes a theoretical framework to explain PCTs observed during an oceanographic cruise in the Mediterranean Sea. We consider both a homogeneous and a variable environment, respectively corresponding to the waters on both sides of a front and to the frontal area itself. In the model, PCTs between one community of smaller phytoplankton and one community of bigger phytoplankton are controlled by nutrient supply, but not directly: nutrient supply affects all compartments of the model and creates PCTs by combining bottom-up and top-down controls. This mechanism is observed for both constant (i.e., within a water mass) and pulsed (i.e., in the front) nutrient supply. These results are consistent with *in situ* observations of biomass proportion across a front. This theoretical framework helps to better understand and plan *in situ* observations in oceanic regions characterized by fine-scale dynamics and oligotrophic conditions.

1. Introduction

Understanding phytoplankton behaviour and biodiversity is crucial due to their pivotal role in the biological sequestration of carbon and in controlling the ecological structure of the ocean (Frederiksen et al., 2006). Phytoplankton exhibit vast diversity in shapes, sizes, species and ecological traits, which impacts ocean biogeochemistry and contributes to the stability of ecosystems (Dutkiewicz et al., 2020). Oligotrophic regions (i.e., 60% of the ocean surface (Longhurst, 1998)) represent the planet's largest cohesive ecosystems (Moutin et al., 2017) and are set to expand with future warming (Polovina et al., 2008). Small phytoplankton, which dominate the trophic base of oligotrophic regions, are expected to be further favoured by rising temperatures (Morán et al., 2010). While oligotrophic regions are nutrient-poor and low-biomass on average, fine-scale dynamics (1–100 km, days–months) can boost primary production there by 10 to 30% (Lévy et al., 2001) and enhance phytoplankton diversity (Lévy, 2015). As a consequence, understanding phytoplankton dynamics at fine scales in oligotrophic regions is essential in order to predict future changes in carbon sequestration and ecosystem structure.

Fine-scales fronts are created by the encounter between water masses of distinct origins with different characteristics such as temperature and salinity (McWilliams, 2021). Frontal dynamics impact biogeochemistry in 3D by influencing transport, both by acting as horizontal barriers and by creating vertical nutrient fluxes (Mahadevan and Archer, 2000) that support more phytoplankton diversity and biomass (Marra et al., 1990; Li et al., 2012; Lévy et al., 2015; Clayton et al., 2017). The influence of fronts extends beyond themselves as they shape the surrounding environment, marking regions of transition or separation between contrasting water patches (Acha et al., 2015). While several studies have highlighted the importance of fine-scale fronts in affecting biology (e.g. Hitchcock et al., 1993; Yoder et al., 1987; Mahadevan, 2016; Lévy et al., 2018; Mangolte, 2022) the processes at play are still relatively unknown.

One reason is that the small size of fronts, their ephemeral characteristics and uncertain dynamics make them challenging to observe *in situ* (Lévy et al., 2012). Only oceanographic cruises specially designed for fine-scale studies can identify and track plankton patches and their boundaries. A large part of the ocean, characterized by

* Corresponding author.
E-mail address: laurina.oms@mio.osupytheas.fr (L. Oms).

https://doi.org/10.1016/j.jmarsys.2024.104021
Received 4 April 2024; Received in revised form 31 October 2024; Accepted 2 November 2024
Available online 12 November 2024
0924-7963/© 2024 The Authors. Published by Elsevier B.V. This is an open access article under the CC BY license (http://creativecommons.org/licenses/by/4.0/).

oligotrophic conditions and moderate energy, has been understudied. Most fine-scale biological observations were conducted in productive and dynamic regions, such as Western Boundary Currents (WBC) and Eastern Boundary Upwelling Systems (EBUS). Past and recent *in situ* observations in these regions emphasized the mosaic-like nature of the ocean surface, as evidenced by variations in phytoplankton size classes and biomass across frontal areas in the California Current Ecosystem (e.g., Taylor et al., 2012; Li et al., 2012; Gangrade and Franks, 2023). In the equatorial Pacific, large aggregations of diatoms were found within a front (Yoder et al., 1994), and in the Middle Atlantic Bight, increased phytoplankton growth has been linked to nutrient enrichment conditions at fronts (Marra et al., 1990). Nevertheless, the complexity of capturing fine-scale processes requires specialized tools and strategies to achieve sufficient measurement resolution in these areas. Before the SWOT (Sea Water Ocean Topography) satellite launched in 2022, localizing fine-scale structures was challenging. Fine-scale structures could be observed in ocean colour and SST satellite maps, but these measurements are strongly impacted by clouds, and altimetry was cloud-free but too coarse. SWOT dramatically increased altimetry resolution while remaining unaffected by clouds, thus enabling *in situ* sampling to accurately target fine-scale structures of the order of 15 to 30 km (Morrow et al., 2019). An important challenge that this work addresses is the lack of interpretation of pre-SWOT fine-scale observations in oligotrophic areas.

The Mediterranean Sea displays high biodiversity (Bianchi and Morri, 2000) and moderate energy oligotrophic conditions, along with a thermohaline circulation, which make it a miniature model of the global ocean (Bethoux et al., 1999). This contrasts with oceanic areas like WBC or EBUS, where intense dynamics and large nutrient inputs can hide fine-scale coupled dynamics. The Mediterranean Sea oligotrophy is mainly due to the very low concentration of inorganic phosphorus, which is assumed to limit primary production (Moutin and Raimbault, 2002; Siokou-Frangou et al., 2010). The phosphate limitation is driven by a combination of hydrological exchanges, biological processes, and chemical interactions (Moutin and Raimbault, 2002). However, a significant variability in surface phosphate concentrations exists due to physical forcing, such as diapycnal fluxes (Pulido-Villena et al., 2021). The Mediterranean Sea is particularly interesting because, although the phytoplankton community is dominated by picophytoplankton, there is a highly dynamic mosaic of populations that vary on temporal and spatial scales, due in part to its diverse physical structure (Siokou-Frangou et al., 2010). The OSCAHR cruise in the Ligurian Sea (Doglioli, 2015) combined high-resolution measurements of both physical and biological variables, revealing the influence of physical dynamics on the spatial distribution of phytoplankton through cyclonic structure (Marrec et al., 2018). The SHEBEX cruise in the Balearic Sea showed that the Lagrangian properties of the flow have important biological consequences from phytoplankton to high trophic levels (Hernández-Carrasco et al., 2020). The PROTEVSMED-SWOT cruise performed in the south-western Mediterranean Sea showed contrasted phytoplankton communities in two water masses on either side of a front: picophytoplankton (resp. microphytoplankton) were more abundant in the southern (resp. northern) side of the front (Tzortzis et al., 2021).

These studies underscore the intimate connection between fine-scale dynamics and abrupt phytoplankton shifts over relatively limited distances and time, termed here as "phytoplankton community transitions" (PCTs). The presence of PCTs indicates phytoplankton heterogeneity and adaptation to fine-scale dynamics, allowing high diversity even in oligotrophic regions. According to Lévy et al. (2018), three sets of fine-scale processes can explain observed PCTs: (i) passive processes linked to horizontal transport; (ii) active processes linked to vertical transport and (iii) reactive processes linked to biotic interactions, such as zooplankton grazing. Passive processes create so-called fluid dynamical niches (d'Ovidio et al., 2010). Active processes influence nutrient transport, which affects the bottom-up controls on phytoplankton (Clayton et al., 2014) and, consequently, the trophic chain structure (Poggiale et al., 2013). Reactive processes were shown to be another important component in the structuring of phytoplankton communities by several modelling studies (McCauley and Briand, 1979; Mitra et al., 2007; Adjou et al., 2012; Zheng et al., 2022).

In this work we focus on fine-scale frontal dynamics and associated contrasts in phytoplankton abundances and biomass by asking the question: how do fine-scale dynamics explain PCTs? We explore two hypotheses: (i) fronts influence nutrient fluxes through physical processes (bottom-up control), involving both active and passive processes, and (ii) fronts affect biotic interactions, including zooplankton grazing (top-down control), involving the reactive process. We build our scientific questioning on the *in situ* observed contrasted phytoplankton communities identified by Tzortzis et al. (2021). These were linked to contrasted growth and loss rates (Tzortzis et al., 2023), but a comprehensive explanation of the processes associated to these observations is still lacking.

We address these hypotheses by using a simple model of phytoplankton dynamics. Models are powerful tools to investigate processes where *in situ* observations are incomplete. Modelling studies have been essential for investigating and understanding the connections between fine-scale and phytoplankton dynamics (e.g. Franks, 1992; Lévy et al., 2001, 2015; Barton et al., 2010). In addition, model results motivate the implementation of dedicated oceanographic campaigns, play a pivotal role in shaping their strategies, and help bridge the gap between the feasible resolution of *in situ* observations and the small spatio-temporal scales of marine ecosystem dynamics. The coupling between physics and biology has been explored from models with very simple formulations (e.g. Grover, 1990) to great complexity (e.g. Aumont et al., 2015). NPZ (nutrient–phytoplankton–zooplankton) models are a common tool in oceanography for their ability to have simple formulations, few parameters and various applications (Franks, 2002). Due to their low computational cost, 0D NPZ models can quickly test hypotheses across various scenarios, making them valuable for exploring different environmental conditions. This efficiency complements observational data by providing insights that are difficult to capture *in situ*. In this study we used a NPZ model adapted to oligotrophic regions and applied in two scenarios: one with constant forcing simulating homogeneous water masses, and another with pulsed forcing simulating the variable environment of a frontal area. The NPZ model is conceived upon data and results from Tzortzis et al. (2021, 2023), which highlighted significant shifts between two phytoplankton communities. We also conducted further data analysis to enable comparison with the model simulations. The observational data provide essential input for guiding the model, which in turn helps elucidate the mechanisms behind the observed patterns.

The article is structured into three main sections. The Materials and Methods introduce the PROTEVSMED-SWOT cruise, *in situ* biomass calculations, and the NPZ model. The Results section displays findings from both *in situ* data and model simulations, with the latter presented in two parts: constant forcing and pulsed forcing. The Discussion section proposes a theoretical framework for the observed PCTs.

2. Materials and methods

This study combines *in situ* observations with model simulations. We utilize *in situ* data from an oceanographic cruise, in particular flow cytometry measurements, previously analysed by Tzortzis et al. (2021, 2023). Building on these studies, we developed our model and reanalyzed the data by estimating biomass from abundances to enable comparison with the model simulations.

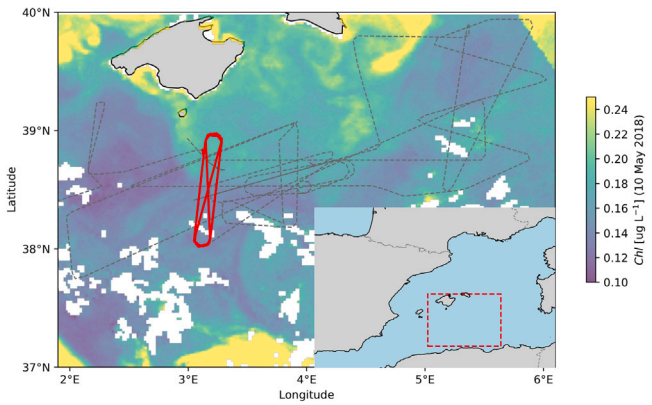

Fig. 1. Surface chlorophyll-a concentrations for 10-May-2018, overlaid by the ship's route. The red segment indicates the sampling from 11-May-2018 to 13-May-2018. The inset map at the bottom of the figure displays the study region, with the red square representing the sampling area.

2.1. In situ cruise and biomass calculation

The PROTEVSMED-SWOT campaign took place aboard the RV Beautemps-Beaupré between 30-April-2018 and 18-May-2018, in the southern Balearic Islands (Dumas, 2018). We crossed a frontal zone that separates different water masses, which were indicated by contrasting satellite chlorophyll concentrations (provided by CLS https://www.cls.fr/, Fig. 1). Using an adaptive Lagrangian sampling strategy and high-resolution data from a CTD sensor mounted on a towed vehicle (SeaSoar), Tzortzis et al. (2021) identified two different water masses separated by a front located at 38.5°N: a colder and saltier one to the north (hereafter "northern water mass") and a warmer and fresher one to the south (hereafter "southern water mass") (Fig. A.10). Each water mass was also characterized by contrasted abundances of nine phytoplankton clusters identified by underway flow cytometry (Tzortzis et al., 2021). Both water masses were continuously sampled along a designated ship route, defining the region as the "hippodrome" between 11-May-2018 and 13-May-2018 (Fig. 1, red part) allowing each water mass to be visited for a total of 24 h (daily cycle). It is important to note that the front was crossed, but no high-resolution samples were performed during the PROTEVSMED-SWOT cruise.

Phytoplankton abundances are reanalyzed here to be expressed in terms of carbon biomass for comparison with the model. Cell carbon content can be estimated from cell biovolume (corresponding to the 3D space occupied by a cell), enabling measured abundances (cell m^{-3}) to be converted into biomass (mmolC m^{-3}) (Menden-Deuer and Lessard, 2000). The biovolume (BioV [μm^3/cell]) was calculated by converting optical measurements by flow cytometry according to Eq. (1a) (Foladori et al., 2008; Marrec et al., 2018; Tzortzis et al., 2023). The carbon content (Q_c [mmolC $cell^{-1}$]) was calculated according to Eq. (1b) (Menden-Deuer and Lessard, 2000). The biomass (BioM [mmolC m^{-3}]) was then calculated for each sample by multiplying phytoplankton measured abundances by their estimated average carbon content. This method was applied to the nine phytoplankton clusters characterized by Tzortzis et al. (2021). For the sake of simplicity, we regrouped the nine clusters into three phytoplankton groups defined by cell size:

1. Picophytoplankton, PICO (<2 μm)
2. Nanophytoplankton, NANO (>2 and <20 μm)
3. Microphytoplankton, MICRO (>20 μm)

$$\text{BioV} = \text{FWS}^{\beta_1} \cdot e^{-\beta_0} \tag{1a}$$

$$Q_c = \alpha_0 \cdot \text{BioV}^{\alpha_1} \tag{1b}$$

$$\text{BioM} = \text{abundance} \cdot \bar{Q}_c \tag{1c}$$

The term "FWS" represents the ForWard Scatter, an optical measurement obtained by flow cytometry that is a proxy of the cell size. β_0 and β_1 are the parameters of the log–log regression between the FWS and the biovolume, with values of $\beta_0 = -5.8702$ and $\beta_1 = 0.9228$ (Tzortzis et al., 2023). The parameters α_0 and α_1 of the log–log regression between biovolume and carbon content are specified as follows: for PICO, $\alpha_0 = 0.210$ and $\alpha_1 = 0.939$; for NANO, $\alpha_0 = 0.260$ and $\alpha_1 = 0.860$; and for MICRO, $\alpha_0 = 0.287$ and $\alpha_1 = 0.811$ (Menden-Deuer and Lessard, 2000).

2.2. Model description

The NPZ model was developed for oligotrophic waters and is applied to the Mediterranean Sea to investigate the observed shift between PICO and MICRO phytoplankton communities across the frontal area. The schematic diagram gives a pictorial view of trophic links between state variables and exchanges with the external environment (Fig. 2). The main assumptions used to construct the equations are as follows: there is only one limiting nutrient, with phosphate (PO_4) being the key limiting nutrient in the Mediterranean Sea (Moutin and Raimbault, 2002). Organic matter dynamics and recycling are fast, meaning that the detrital compartment and storage within the plankton are absent. Dead phytoplankton cells do not sink but are instead recycled directly into the nutrient compartment. The uptake equation approximates Droop's growth model (Droop, 1983) using a Monod function (Monod, 1942). The dynamics of phytoplankton are controlled by two factors: nutrient-limited growth with a single nutrient (bottom-up control) and grazing limitation by a single zooplankton group, which has differential grazing rates on each phytoplankton group (top-down control). The choice of a single nutrient and zooplankton group was made to avoid the effects of nutrient co-limitation (Poggiale et al., 2010) and to maintain simplicity.

The model equations are:

$$\frac{dN}{dt} = N_{supply} + \epsilon_e(1-\gamma)Z\sum g_i + \sum m_{P,i}P_i + \epsilon_n m_n Z - \sum \mu_i P_i \tag{2a}$$

$$\frac{dP_i}{dt} = \mu_i P_i - g_i Z - m_{P,i}P_i \tag{2b}$$

$$\frac{dZ}{dt} = Z\gamma\sum g_i - m_q Z^2 - m_n Z \tag{2c}$$

N stands for nutrient, P stand for phytoplankton class i, and Z stands for zooplankton. All state variables are masses expressed in mmolC m^{-3}, assuming a C:P molar ratio of 130:1 in phytoplankton in P-depleted conditions (Pulido-Villena et al., 2021). We discretized the equations with an Euler's explicit numerical scheme, with a 0.1-day time step.

The growth rate of phytoplankton class i (μ_i [d^{-1}]) is calculated from a Monod function:

$$\mu_i = \frac{N}{N + K_{P,i}}\mu_{max,i} \tag{3}$$

The grazing rate of zooplankton on phytoplankton class i (g_i [d^{-1}]) is calculated according to the Holling type II response :

$$g_i = \frac{P_i}{P_1 + P_2 + K_{Z,i}}g_{max,i} \tag{4}$$

The detailed definitions of all parameters are provided in Table 1. Parameter values were chosen based on the literature. The two phytoplankton size classes were parameterized to represent picophytoplankton (P_1) and microphytoplankton (P_2). P_1, as a community of small species, is specialized in nutrient uptake in low-nutrient conditions ($K_{P,1} < K_{P,2}$) while P_2, as a community of larger species, is specialized in defence against predators ($g_{max,1} > g_{max,2}$). This implies that P_1 should dominate the community in nutrient-poor waters and P_2 should dominate the community in nutrient-rich waters (Thingstad and Rassoulzadegan, 1999; Bohannan and Lenski, 2000).

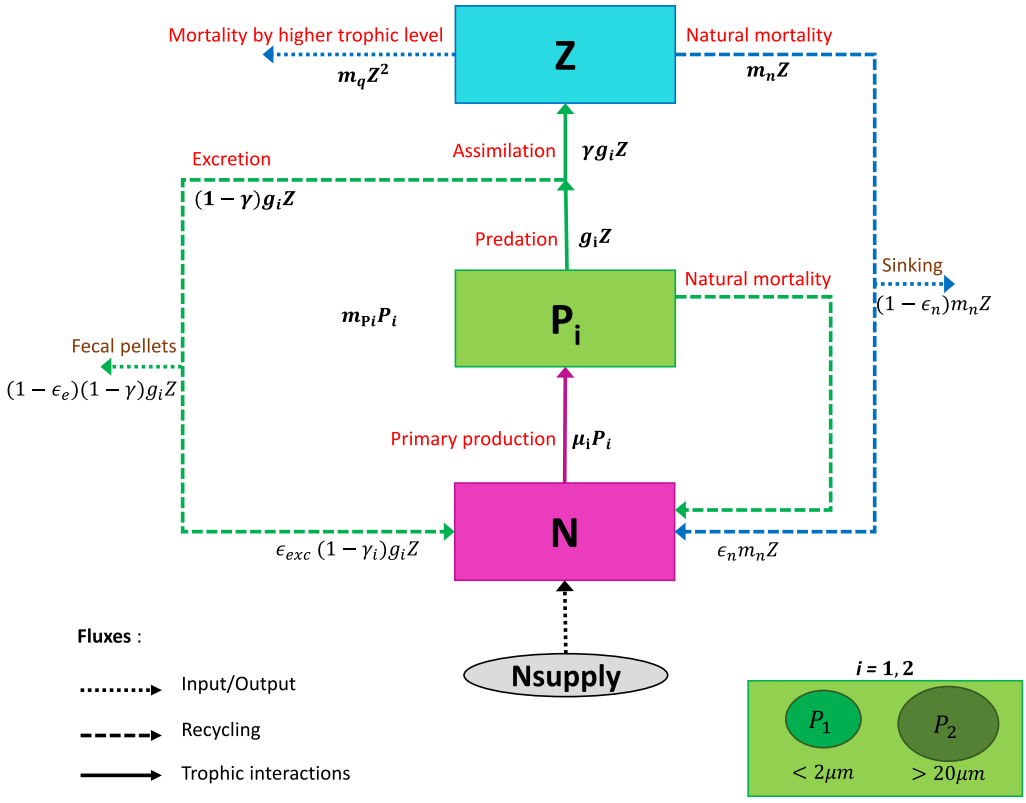

Fig. 2. Model diagram. Model state variables are represented by boxes, biochemical processes by arrows and external forcing by an ellipse. All state variables are masses expressed in mmolC m^{-3}. Note that the colour code: magenta for N, light green for P_1, dark green for P_2 and cyan for Z, is used throughout this paper.

Table 1
Model parameters with units, associated values and references.

Symbol	Definition	Unit	Value	Reference
$\mu_{max,1}$	P_1 maximum growth rate	d^{-1}	1.9872	Baklouti et al. (2021)
$\mu_{max,2}$	P_2 maximum growth rate	d^{-1}	2.7648	Baklouti et al. (2021)
$g_{max,1}$	Z maximum grazing rate on P_1	d^{-1}	3.89	Auger et al. (2011)
$g_{max,2}$	Z maximum grazing rate on P_2	d^{-1}	0.43	Auger et al. (2011)
$K_{P,1}$	P_1 half-saturation constant	mmolC m^{-3}	1	This article
$K_{P,1,litt}$	Half-saturation constant of *Synecho.* and small phyto resp.	mmolC m^{-3}	1.82, 6.5	Timmermans et al. (2005) and Munkes et al. (2021)
$K_{P,2}$	P_2 half-saturation constant	mmolC m^{-3}	3	This article
$K_{P,2,litt}$	Half-saturation constant of *A. formosa* and diatoms resp.	mmolC m^{-3}	2.6, 13	Grant (2014) and Munkes et al. (2021)
$K_{Z,1}$	Z half-saturation constant for P_1	mmolC m^{-3}	5	Auger et al. (2011)
$K_{Z,2}$	Z half-saturation constant for P_2	mmolC m^{-3}	20	Auger et al. (2011)
$m_{P,1}$	P_1 mortality rate	d^{-1}	0.10	This article
$m_{P,1,litt}$	Mortality rate of P_1 in literature	d^{-1}	0.07, 0.16	Baklouti et al. (2021) and Auger et al. (2011)
$m_{P,2}$	P_2 mortality rate	d^{-1}	0.2	This article
$m_{P,2,litt}$	Mortality rate of P_2 in literature	d^{-1}	0.1, 0.10	Baklouti et al. (2021) and Auger et al. (2011)
m_n	Z natural mortality rate	d^{-1}	0.10	Auger et al. (2011)
m_q	Z quadratic mortality rate	m^3(mmolC d)$^{-1}$	0.061	Auger et al. (2011)
γ	Conversion coefficient from P to Z	–	0.6	Auger et al. (2011)
ϵ_n	Z natural mortality recycling coefficient	–	0.3	This article
ϵ_e	Z excretion recycling coefficient	–	0.7	Baklouti et al. (2021)
N_{supply}	Nutrient supply	mmolC m^{-3} d^{-1}	/	/

N_{supply} is the only external forcing in this study (Eq. (2a)). A total phosphate supply in the south-western Mediterranean Sea of 2.10^{-4} mmolP m^{-3} d^{-1} was estimated during the 2017 PEACETIME cruise (Guieu and Desboeufs, 2017), corresponding to 0.03 mmolC m^{-3} d^{-1} (Pulido-Villena et al., 2021). Given the limited availability of other *in situ* measurements in our study region, we assumed a N_{supply} range from a nutrient-poor to a nutrient-rich water mass between 0.01 and 0.10 mmolC m^{-3} d^{-1}, respectively.

2.3. Analysis

We conducted two analyses of the NPZ model. The first analysis focuses on constant forcing, examining equilibrium at steady state. This helps to elucidate factors influencing PCTs in each sampled water mass on either side of the frontal area, assuming a homogeneous environment with a constant nutrient supply. In the second analysis the model is no longer in steady state and instead focuses on pulsed forcing, examining the response of the state variables after a perturbation. This helps to elucidate the factors influencing PCTs in a simulated variable environment, by considering a frontal system and assuming a pulsed phosphate supplies associated with ageostrophic vertical velocities and/or turbulent mixing enhanced by frontal dynamics (Mahadevan and Archer, 2000; McWilliams, 2021).

The software developed for this work, containing the NPZ model as well as all the calculations mentioned below, is available at: https://github.com/OmsLaurina/toolbox_growthmodel.

2.3.1. Constant forcing

For the steady state analysis (i.e., constant forcing, with value of N_{supply} between 0.01 and 0.1 mmolC m^{-3} d^{-1}), we analysed the model using a simpler version to understand its qualitative behaviour, specifically focusing on the role of N_{supply}. This simplified formulation was achieved by assuming that concentrations are small relative to half-saturation constants i.e., $N \ll K_{P,i}$ so that $N + K_{P,i} \simeq K_{P,i}$, which lets us approximate equations by removing the variable denominator in the growth rate and grazing rate functions (Eqs. (5) and (6)).

Eq. (3) becomes:

$$\mu_i = \frac{N}{K_{P,i}} \mu_{max,i} \tag{5}$$

Eq. (4) becomes:

$$g_i = \frac{P_i}{K_{Z,i}} g_{max,i} \tag{6}$$

Equilibrium state was reached, following a 2000-day simulation, with constant forcing value of N_{supply} (between 0.01 and 0.1 mmolC m^{-3} d^{-1}). For both the simplified and full models we determined analytical steady state solutions, except in cases of coexistence of P_1 and P_2 , where the solutions are obtained numerically by running 2000-day simulations (Fig. B.14).

The stability of steady state solutions was analysed for the simplified and full models by calculating the Jacobian matrices associated with these solutions. The dominant eigenvalue of the matrices (complex number, termed λ_{max}) indicates the stability with which perturbations propagate around an equilibrium. If the real part of the dominant eigenvalues is negative, the equilibrium is stable, if not the equilibrium is unstable. The calculation of eigenvalues for different values of N_{supply} within the range defined above, were then used to construct bifurcation diagrams, enabling us to explore how equilibria interact and evolve with different values of N_{supply}.

We evaluated bottom-up forcing on the model outputs using simulations with varying N_{supply} values and top-down forcing with simulations with varying grazing configurations. Grazing configurations were: first, excluding grazing ("no grazing test", $Z = 0$), second, identical predation ("equal grazing test", with parameters based on P_1 , i.e. $g_{max,1} = g_{max,2} = 3.89$ d^{-1}, $K_{Z,1} = K_{Z,2} = 5$ mmolC m^{-3}, and third, differential predation (default configuration, see Table 1).

Full model sensitivity to parameters under constant forcing was tested following the method used by Messié and Chavez (2017). We examined the effect of varying values of $u_{max,i}, K_{P,i}, g_{max,i}$ and $K_{Z,i}$, as these parameters dictate bottom-up and top-down forcing on each phytoplankton, ultimately controlling their relative proportions. For each parameter, three runs were performed: first, we used the default parameter value (Table 1); second, half of the default value; and third, twice the default value (others parameters were maintained at their default value). The percentage of variation represents the difference between the outcomes of the third and second runs, divided by the result of the first (average value of the last 200 values in a 2000-day simulation). A positive variation percentage signifies the second run's value is higher than the third run's value, while a negative percentage indicates the opposite. This analysis was conducted for the two values of N_{supply} defining the nutrient-poor (N_{supply} = 0.01 mmolC m^{-3} d^{-1}) and nutrient-rich (N_{supply} = 0.10 mmolC m^{-3} d^{-1}) water masses for a total of 8 (parameters) x3 (runs) x2 (N_{supply}) simulations. Figs. B.16 and B.17 in the Appendices show the temporal evolution of state variables at each runs.

2.3.2. Pulsed forcing

To simulate fluctuating forcing within a front, a pulsed N_{supply} was implemented as:

$$N_{supply}(t) = b \cdot (U(t - t_1) - U(t - t_2)) + N_{supply,0} \tag{7}$$

where b is the amplitude of the pulse, t_1 and t_2 are respectively the start and end time of the pulse, and $N_{supply,0}$ is the value of N_{supply} at $t = 0$. U(x) is the step function (or Heaviside function) defined as:

$$U(x) = \begin{cases} 0 & \text{if } x < 0 \\ 1 & \text{if } x \geq 0 \end{cases}$$

We investigated the effect of amplitude and number of pulses on the temporal evolution of the state variables. The analysis started with the coexistence of both phytoplankton species in equivalent proportion, obtained with $N_{supply}, 0$.

3. Results

3.1. In situ observations

Fig. 3 displays the biomass of phytoplankton groups presenting a clear contrast across latitude 38.5°N, which was identified as the position of a front between two water masses of different origins (Tzortzis et al., 2021). The biomass contrast across the front was quantified for each phytoplankton size group by calculating the ratio $f_{BioM,j}$ between the average biomass south ($BioM_{S,j}$ [mmolC m^{-3}]) and north ($BioM_{N,j}$ [mmolC m^{-3}]) of the front (Eq. (8)). If $f_{BioM,j} > 1$ the biomass in the south is greater than the biomass in the north, and vice versa if $f_{BioM,j} < 1$.

$$f_{BioM,j} = \frac{\overline{BioM_{S,j}}}{\overline{BioM_{N,j}}} \tag{8}$$

where $j = PICO, NANO, MICRO$.

The result indicates that the PICO group was more represented in southern waters ($f_{BioM,PICO} > 1$), while the MICRO group was more represented in northern waters ($f_{BioM,MICRO} < 1$) (Fig. 3). Patterns were inconsistent between the 2 subgroups comprising the NANO group: NANO1 was higher south of the front ($f_{BioM,NANO1} = 1.6$), while the larger NANO2 remained similar on both sides of the font ($f_{BioM,NANO2} = 1.0$) (Fig. A.11). The lack of contrast for NANO across the front justifies our choice of parameterizing the model based on PICO and MICRO. In the following P_1 was considered to represent both NANO1 and PICO, and P_2 the remaining groups (MICRO and NANO2).

3.2. Numerical simulations with constant forcing

Analytical calculations and numerical simulations were carried out to study the stability of the model equilibria. Fig. 4 shows the bifurcation diagrams for both the simplified and full models. With the simplified model (Fig. 4a.) we analytically found two equilibria, each one corresponding to the absence of one of the two phytoplankton groups. The first equilibrium $\bar{X}_1$ ($P_2 = 0$) is stable up to a value of N_{supply} of 0.055 mmolC m^{-3} d^{-1} (i.e. the bifurcation point), while the second equilibrium $\bar{X}_2$ ($P_1 = 0$) is unstable up to 0.055 mmolC m^{-3} d^{-1}. This bifurcation, where two equilibrium points exchange stability as parameters change, is called a "transcritical bifurcation". Using the full model (Fig. 4b.), we analytically identified two equilibria, each associated with the absence of one of the two phytoplankton groups. The first equilibrium $\bar{Y}_1$ ($P_2 = 0$) is stable up to a value of N_{supply} of 0.140 mmolC m^{-3} d^{-1} (i.e bifurcation point), while the second equilibrium $\bar{Y}_2$ ($P_1 = 0$) is never stable. Additionally, we numerically determined one equilibrium representing the coexistence of both phytoplankton groups. The coexistence equilibrium is always stable, but negative for $N_{supply} < 0.045$ mmolC m^{-3} d^{-1} (irrelevant to our investigation). The positive equilibrium is achieved when N_{supply} exceeds 0.045 mmolC m^{-3} d^{-1}.

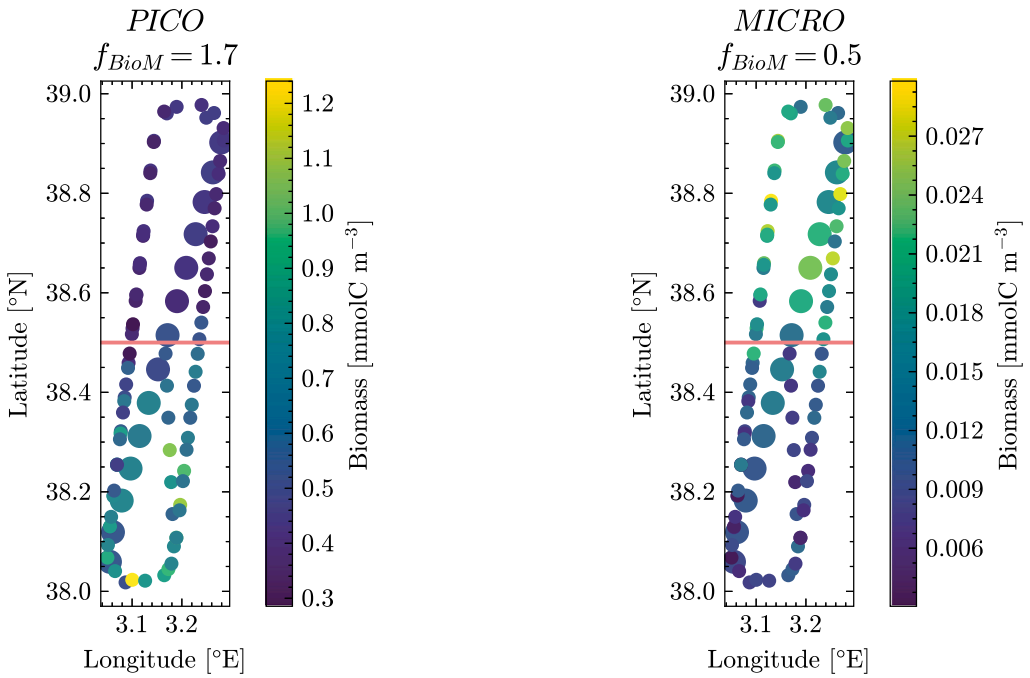

Fig. 3. *In situ* measurements of PICO (left panel) and MICRO (right panel) biomass across the 'hippodrome' sampling segment during the PROTEVSMED-SWOT campaign. The coral line represents the estimated position of the front. The value of the biomass factor $f_{BioM,j}$ of each group is reported at the top of each subplot. The larger dots represent the transect analysed by Tzortzis et al. (2021) and corresponding to the sampling period 11-May-2018 02:00 to 11-May-2018 08:40.

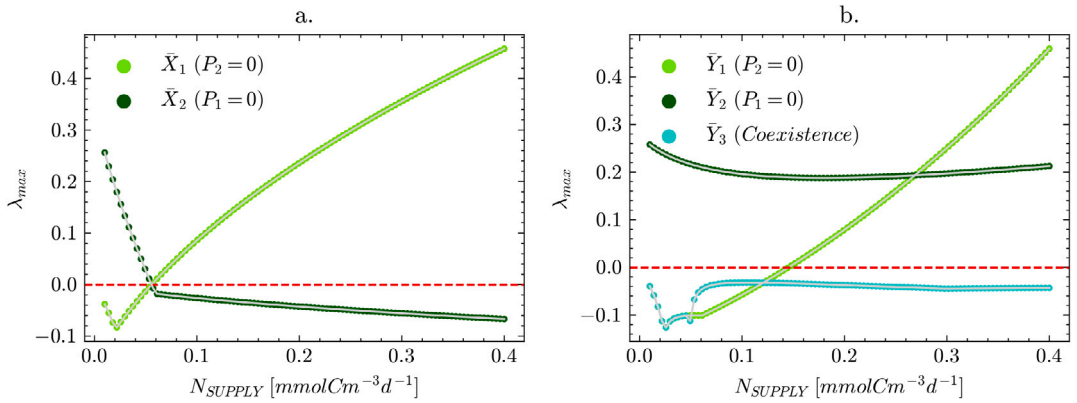

Fig. 4. Bifurcation diagrams representing the dominant eigenvalue λ_{max} calculated for nutrient supply N_{supply} ranging between 0.01 and 0.40 mmolC m^{-3} d^{-1}. Panel a. shows the results of the simplified model: the light green line represents the first equilibrium ($\bar{X}_1$) and the dark green line represents the second equilibrium ($\bar{X}_2$). Panel b. shows the results of the full model: the light green line represents the first equilibrium ($\bar{Y}_1$), the dark green line represents the second equilibrium ($\bar{Y}_2$) and the turquoise line represents the third equilibrium ($\bar{Y}_3$). The dotted red lines represent $\lambda_{max} = 0$. Equilibria are stable when curves are below this red line ($\lambda_{max} < 0$), and unstable when curves are above this red line ($\lambda_{max} > 0$). Bifurcation points correspond to the intersection between the curves and the red line.

3.2.1. Bottom-up vs. top-down controls

We explored the role of bottom-up and top-down controls by calculating the equilibrium values of the system after 2000 days of simulations within the N_{supply} range from 0.01 to 0.10 mmolC m^{-3} d^{-1} (Fig. B.14), and defining the R-ratio as:

$$0 \leq R = \frac{P_1}{P_1 + P_2} \leq 1 \tag{9}$$

By definition R-ratio is equal to 0 if $P_1 = 0$ and equal to 1 if $P_2 = 0$.

Fig. 5 shows the Monod curves representing the phosphate uptake kinetics of P_1 and P_2. The growth rate of P_2 is higher than for P_1 only for $PO_4 > 0.03$ mmolP m^{-3}. This implies that PCTs would happen at unrealistic high nutrient concentrations not only higher than represented by the model (shaded area) but also higher than measured *in situ* concentrations (dashed red line) (Pulido-Villena et al., 2021).

The "no grazing test" demonstrates the importance of the presence of zooplankton for observing PCTs. Without zooplankton grazing, P_1 increases indefinitely, no equilibrium is reached and R-ratio is always equal to 1 (Fig. B.12). With the same grazing pressure on both phytoplankton groups, we obtained an equilibrium, but no coexistence. Indeed, P_2 disappears very rapidly and R-ratio becomes equal to 1 (Fig. B.13). These tests demonstrate that differential grazing is necessary to reach equilibria with P_2 survival (R-ratio < 1).

Fig. 6 shows the influence of N_{supply} on system equilibria using the R-ratio and now considering the differential grazing pressure. With low (resp. high) values of N_{supply} , P_1 (resp. P_2) largely dominates and R-ratio tends to 1 (resp. 0). The transition point, i.e. the value of N_{supply} where R-ratio = 0.5, is reached for N_{supply} equal to 0.050 mmolC m^{-3} d^{-1}. Note that all state variables increase with N_{supply} .

3.2.2. Sensitivity analysis

Fig. 7 illustrates the model's sensitivity to each of the model's main parameters. This is represented by the relative variation of each

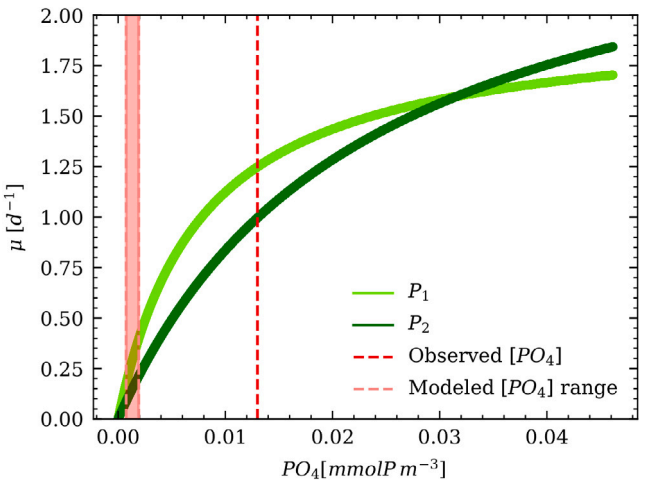

Fig. 5. Theoretical Monod curves representing the growth rates of P_1 and P_2 as a function of N concentration. The shaded area in light red depicts the portion of Monod curves that is constrained by model-predicted values of N_{supply} ranging from 0.01 to 0.10 mmolC m^{-3} d^{-1}, the resulting concentrations of N range from 7.10^{-4} to 0.002 mmolP m^{-3}. The dashed line in dark red corresponds to the average concentration of 0.013 mmolP m^{-3} measured by Pulido-Villena et al. (2021) in the south-western Mediterranean Sea.

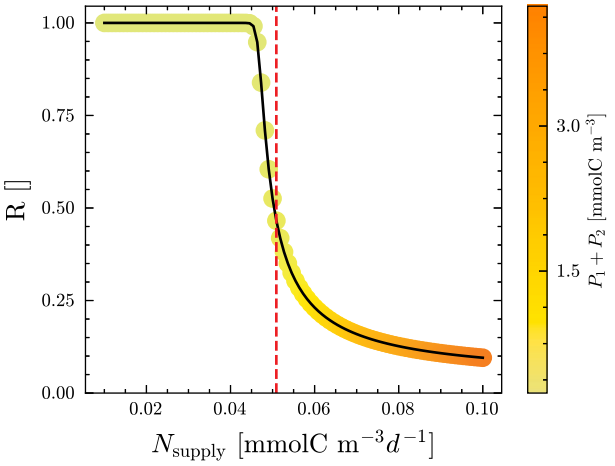

Fig. 6. R-ratio as a function of different values of N_{supply} . The colour bar represent the total biomass ($P_1 + P_2$). The dashed red line corresponds to the value of N_{supply} where the R-ratio is closest to 0.5 (i.e. when P_1 and P_2 are in close proportions), and the dotted grey line correspond to the phosphate supply measured by Pulido-Villena et al. (2021).

state variable N, P_1 and P_2, as well as the derived variable R-ratio, as a function of changes in parameter values. N_{supply} being the only external forcing, we separate the figure in two plots corresponding to the extreme values of N_{supply} used in this work. Z is not displayed in the figure because its steady state value results from the equilibrium between N_{supply} and the three sink terms (fecal pellets, sinking and quadratic mortality) that are controlled by parameters not investigated in Fig. 7.

For low values of N_{supply} (left panel), the relative variation of N is positive for $K_{P,1}$ and $g_{max,1}$ and negative for $\mu_{max,1}$, which is the most sensitive parameter, and $K_{Z,1}$. By contrast, the relative variation of P_1 is negative for $g_{max,1}$ and positive for $K_{Z,1}$. For high values of N_{supply} (right panel), N and P_1 generally show a much lower sensitivity with respect to P_2 and, as a consequence, R-ratio. The relative variation of P_2 is mainly negative for $\mu_{max,1}$ and $K_{P,2}$. R-ratio is sensitive to all parameters except $g_{max,2}$ and $K_{Z,2}$; the others parameters generate variations of over 1000%, i.e. 20 times more than the default value. Details of each parameter's effect for each run are outlined in Figs. B.16 and B.17. Oscillations around the equilibrium value were observed for N when $P_{supply} = 0.1$ mmolC m^{-3} d^{-1} (Fig. B.17).

3.3. Pulsed forcing

To simulate the frontal region, where the 3D fine-scale dynamics can generate vertical nutrient injections, we introduced one to three N_{supply} pulses with varying intensities and we analysed state variables and the R-ratio over a 90-day simulation. Initial conditions were set to the model steady state outputs corresponding to P_1 and P_2 coexisting in equivalent proportion ($P_{supply,0} = 0.050$ mmolC m^{-3} d^{-1}, Fig. 6).

PCTs were observed for moderate pulsed fluxes and/or multiple pulses (i.e., all situations except for the case of a single very weak pulse), with P_2 becoming dominant over time. For all three simulations (from one to three pulses), N increases after each pulse and then sharply decreases as it is consumed by phytoplankton (Fig. 8, top panels). At the end of the simulations, both phytoplankton groups still coexist, but P_2 is dominant. The dominance by P_1, as summarized by the R-ratio, depends on the pulse amplitude (Fig. 8, middle panels). However, the timing of transitions remains similar across a range of pulse amplitudes: P_1 dominates until about 20 days, with a peak concentration just after N_{supply} pulses, then the system switches from P_1 to P_2 from 20 to 40 days. The presence of additional pulses shortens the transition phase, leading to stronger P_2 dominance, while P_1 tends to return to its initial concentration (Fig. 8, middle and top panels). Zooplankton biomass is always maximum during the periods of transition from P_1 to P_2 (Fig. 8, bottom panels). The minimum R-ratio value and the maximum Z biomass achieved after pulses are both enhanced with increasing pulse amplitude.

4. Discussion

The cytometry measurements conducted during the PROTEVSMED-SWOT cruise showed contrasted phytoplankton abundances in two distinct water masses (Tzortzis et al., 2021, and Fig. 3). Here, we developed a NPZ model based on the observed contrasts to understand the community dynamics and better explain the observations. We categorized the phytoplankton into two size groups: small phytoplankton P_1 and large phytoplankton P_2. We hypothesized that fine-scale dynamics, involving hydrodynamic barriers and variations in phosphate flux pulses, generate spatial and temporal PCTs on P_1 and P_2. We considered two scenarios: a homogeneous environment representing distinct water masses on each side of the front (Section 4.1) and a variable environment representing the narrow frontal area separating the two water masses (Section 4.2). From the *in situ* data we calculated the biomass factor (f_{BioM}) and the *in situ* R-ratio, which provide a more detailed quantification of biomass change along the hippodrome transects, allowing comparison with the model output for the homogeneous environment scenario. In the following, we successively consider hypotheses of bottom-up and top-down controls on PCTs in each scenario.

4.1. Driving mechanisms in homogeneous environments

Our simulations show that N_{supply} drives PCTs (Figs. 4 and 6). A bottom-up control via changes in nutrient fluxes thus seems like a logical hypothesis to explain PCTs. However, Monod curves indicate that increased N_{supply} within a realistic range for the oligotrophic ocean promotes P_1 growth but does not allow PCTs (Fig. 5, shaded red area). Note that the modelled N concentrations are lower than observed, possibly due to the absence of a detrital compartment in the model (Edwards, 2001). Grover (1990) demonstrated in a nutrient–phytoplankton model that homogeneous environments are always entirely dominated by the species with the lowest resource requirements. However, our model results and field observations suggest a more

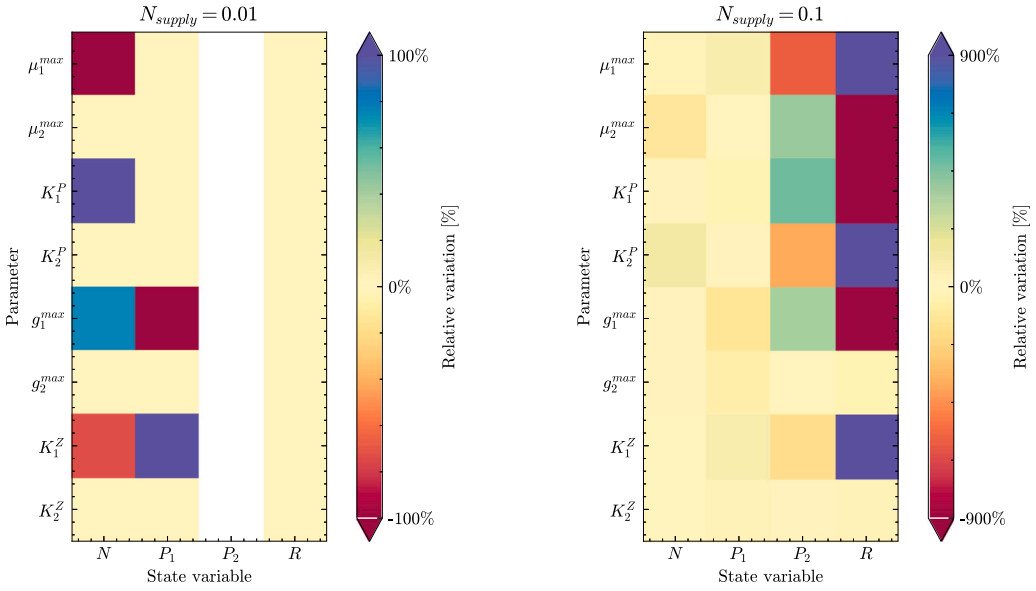

Fig. 7. Sensitivity analysis of key parameters on state variables. The left panel corresponds to the simulations with N_{supply} equal to 0.01 mmolC m^{-3} d^{-1}, and the right panel corresponds to the simulations with N_{supply} equal to 0.10 mmolC m^{-3} d^{-1}. The colours represent the percentage of the relative variation from the default value of the state variables. The white colour for P_2 represents NaN values due to division by 0 (P_2 is equal to 0 for all runs at N_{supply} equal to 0.01 mmolC m^{-3} d^{-1}).

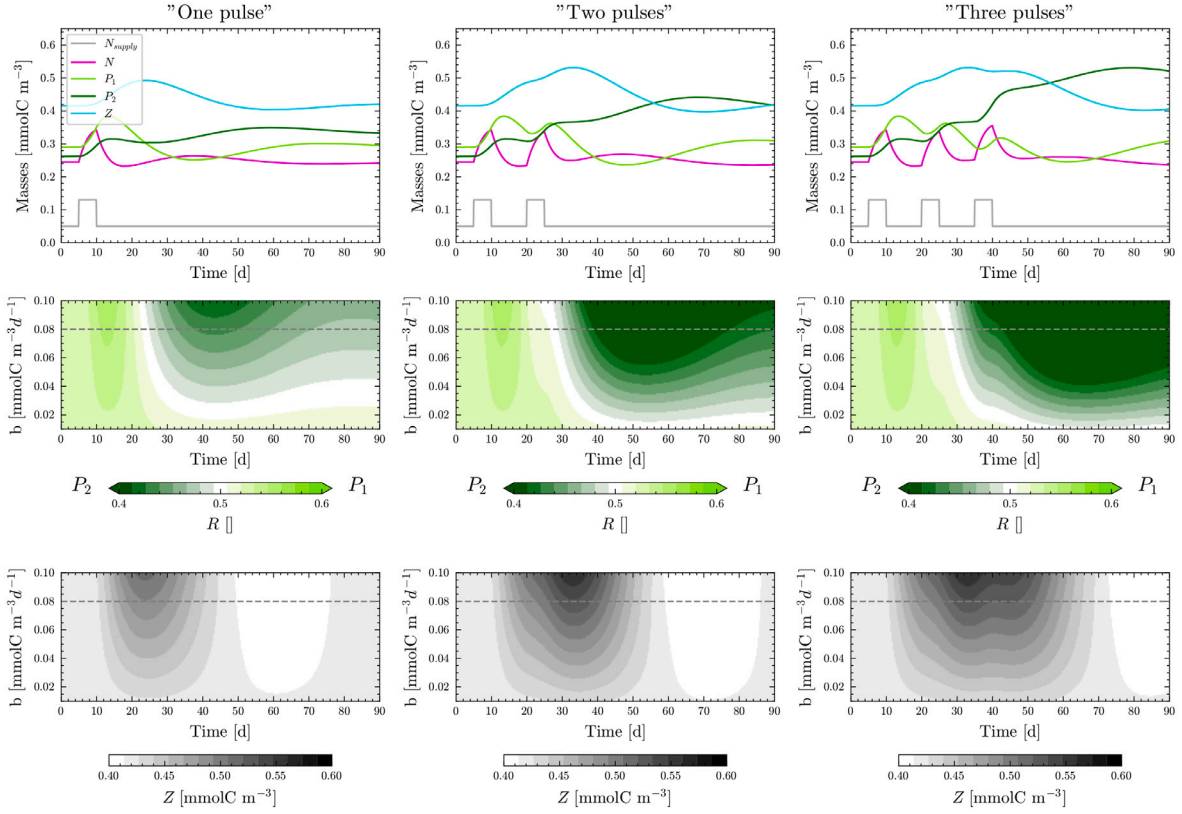

Fig. 8. Response of state variables and R-ratio to a different number of pulses and different amplitudes of N_{supply} over 90-day simulations. The results of the simulations with one, two and three pulses are shown in the left, middle and right columns, respectively. The upper row shows the time evolution of state variables for a pulse amplitude $b = 0.08$ mmolC m^{-3} d^{-1}. The middle row shows the R-ratio as a function of the time and the pulse amplitude. The bottom row is the same as the middle one but for Z. The dotted grey lines correspond to the simulation with a pulse amplitude $b = 0.08$ mmolC m^{-3} d^{-1}.

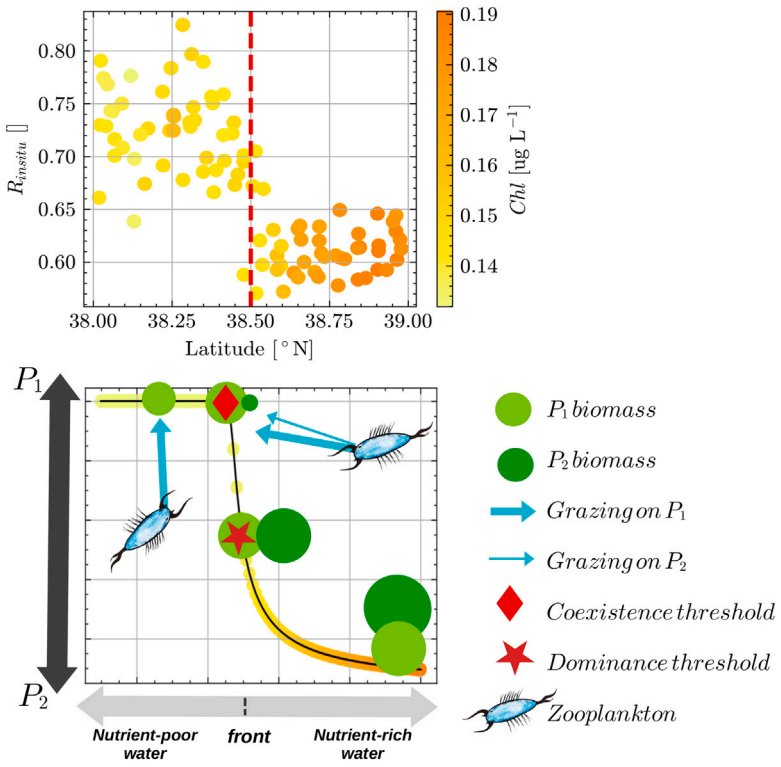

Fig. 9. Top panel: the *in situ* R-ratio, calculated by dividing the biomass of the PICO and NANO1 cytometry groups by the total biomass at each measured points, is plotted as a function of the latitude. The colours represent the chlorophyll concentrations. The dotted red line represents the position of the frontal area (Tzortzis et al., 2021). Bottom panel: the schematic illustrates the proposed mechanism explaining the observed phytoplankton distribution in the two adjacent water masses.

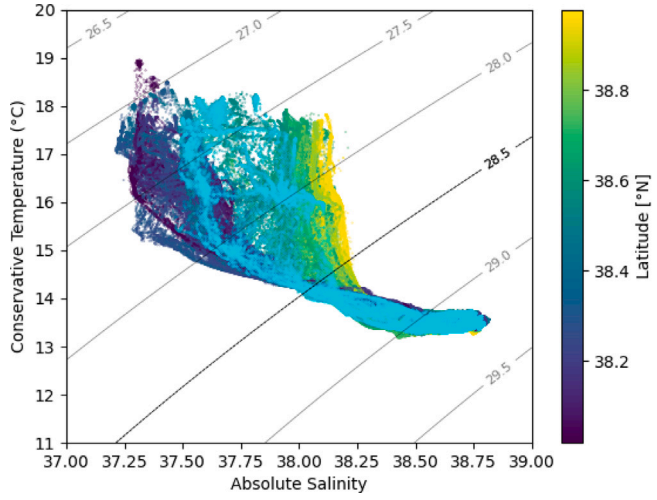

Fig. A.10. Temperature-Salinity diagram of data collected along the hippodrome transects from May 11 to May 13. The colour bar represents latitude. The front, marked in cyan, corresponds to a latitude of 38.5°N (Tzortzis et al., 2021).

frequent occurrence of coexistence with a switch in dominance rather than competitive exclusion. Taken together, these results indicate that the observed PCTs on either side of the front cannot be solely attributed to bottom-up control.

Therefore, we explored the top-down process of zooplankton grazing. Top-down processes were explored by running experiments with no grazing or equal grazing. We found that grazing was necessary for our model to reach equilibrium, leading to stable concentrations and the coexistence of P_1 and P_2. Grazing is known to play a pivotal role in stabilizing the model and allowing coexistence, while nutrient limitation restrain coexistence (Ward et al., 2014). When grazing rates are equal, the model only attains one equilibrium, resulting in the complete dominance of P_1 (Fig. B.13).

To reproduce the observed PCTs, differential grazing rates need to be introduced. Different grazing forcing configurations are a key factor in creating phytoplankton successions and structuring communities during blooms (Prowe et al., 2012). The simplified model (including differential grazing) shows a transcritical bifurcation for N_{supply} equal to 0.055 mmolC m^{-3} d^{-1} (Fig. 4a.). This latter value, identified analytically, is called the "dominance threshold". A similar value of 0.050 mmolC m^{-3} d^{-1} was found numerically for the full model (Figs. 4b. and 6). With the full model we also identified a threshold value of 0.045 mmolC m^{-3} d^{-1}, called the "coexistence threshold", above which both phytoplankton coexist in the system. These results show that differential grazing is key to obtaining PCTs, and that N_{supply} is the main control parameter. This means that, in a homogeneous environment, PCTs are determined by the interplay of bottom-up and top-down controls.

4.2. Driving mechanisms in a variable environment

To assess the effectiveness of combined bottom-up and top-down controls in a variable environment, we simulated pulsed nutrient fluxes. Our results show that one or multiple pulses generate temporal successions between P_1 and P_2 leading to both short-term and delayed temporal PCTs (Fig. 8). This is consistent with freshwater systems where nutrient pulses also cause different species-dependent responses in the phytoplankton community (Yamamoto and Hatta, 2004). The temporal transitions between P_1 and P_2 are linked to the pulse characteristics, such as the amplitude and the number of pulses. We can then transpose our results to the case of fine-scale frontal areas, where the predominance of fast-growing groups like P_2 is explained by nutrient enrichment (Mangolte et al., 2023). However, because the dominance threshold coincides with the zooplankton peak, we attribute the end-of-simulation dominance of P_2 to the "shared predator" concept

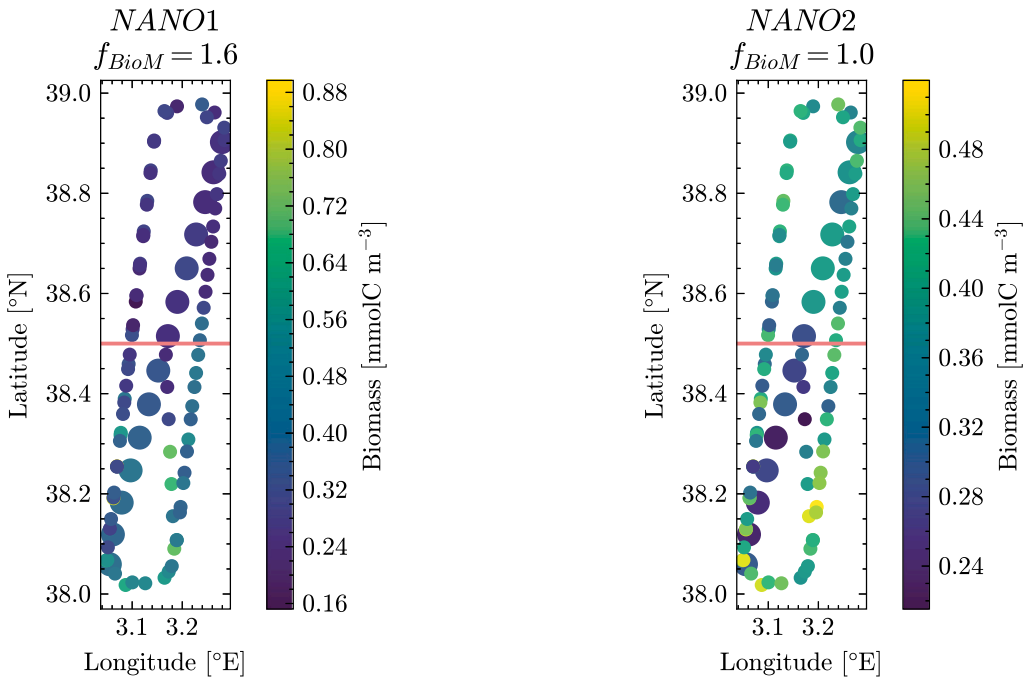

Fig. A.11. *In situ* measurements of NANO1 (left panel) and NANO2 (right panel) biomass across the hippodrome during the PROTEVSMED-SWOT campaign. The coral line represents the estimated position of the front. The value of the biomass factor $f_{BioM,j}$ of each group is reported at the top of each subplot. The larger dots represent the transect shown by Tzortzis et al. (2021) and corresponding to the sampling period 11-May-2018 02:00 to 11-May-2018 08:40.

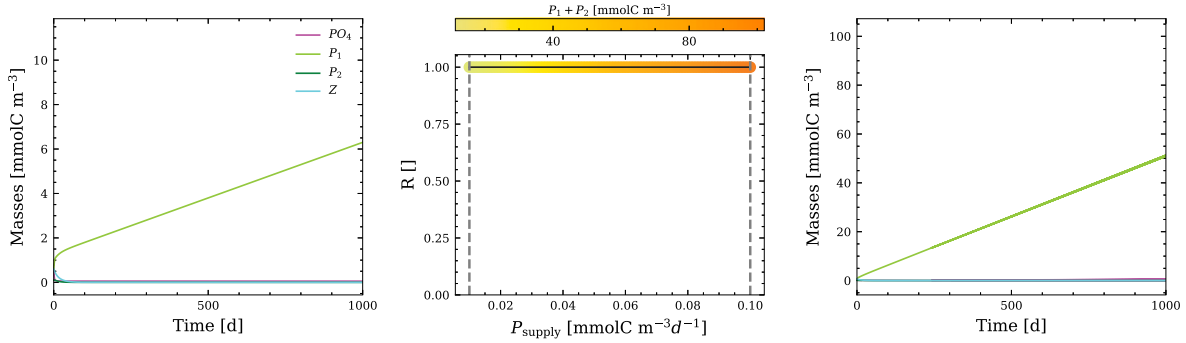

Fig. B.12. Temporal evolution of state variables and R-ratio as a function of different values of N_{supply} for the "No grazing" test. The middle panel shows the evolution of the R ratio as a function of the range of N_{supply} values. The left and right panels show the temporal variation of state variables for a specific N_{supply} value of 0.01 mmolC m^{-3} d^{-1} (left) and 0.10 mmolC m^{-3} d^{-1} (right), indicated by the grey dotted line in the middle graphs.

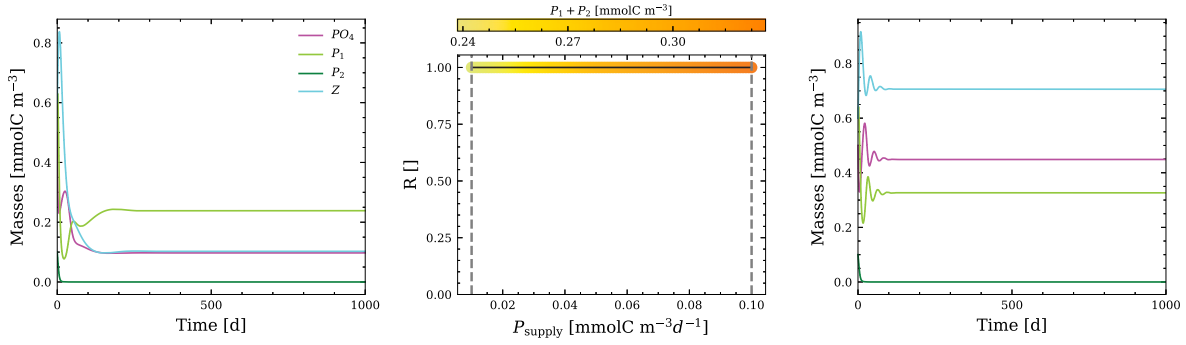

Fig. B.13. Temporal evolution of state variables and R-ratio as a function of different values of N_{supply} for the "Equal grazing" test. The middle panel shows the evolution of the R ratio as a function of the range of N_{supply} values. The left and right panels show the temporal variation of state variables for a specific N_{supply} value of 0.01 mmolC m^{-3} d^{-1} (left) and 0.10 mmolC m^{-3} d^{-1} (right), indicated by the grey dotted line in the middle graphs.

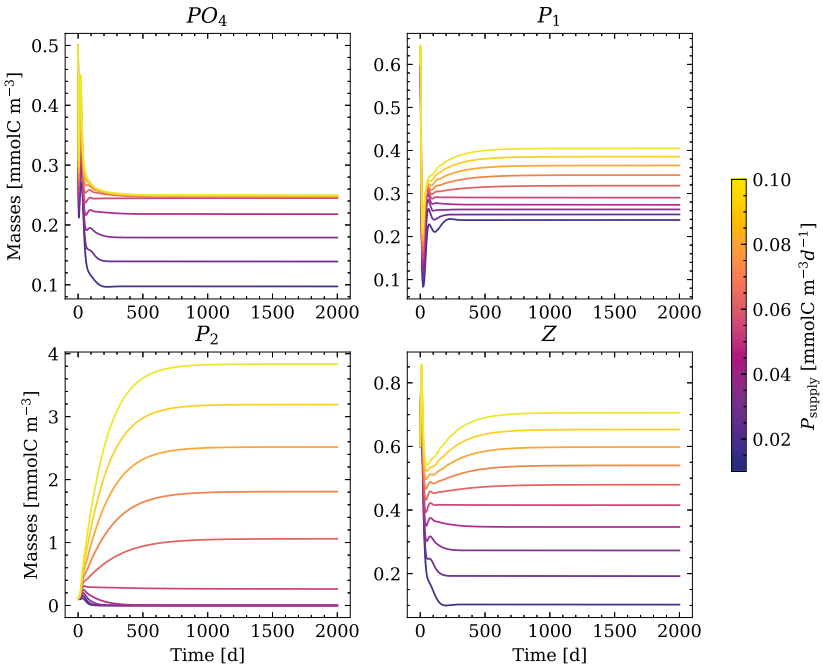

Fig. B.14. Temporal evolution of individual state variables, with lines colour-coded based on their forcing parameter (N_{supply}), ranging from 0.01 to 0.10 mmolC m^{-3} d^{-1} in 10 increments. Simulations are initiated from the following set of values : $N = 0.5$, $P_1 = 0.6$, $P_2 = 0.1$, $Z = 0.6$ [mmolC m^{-3}].

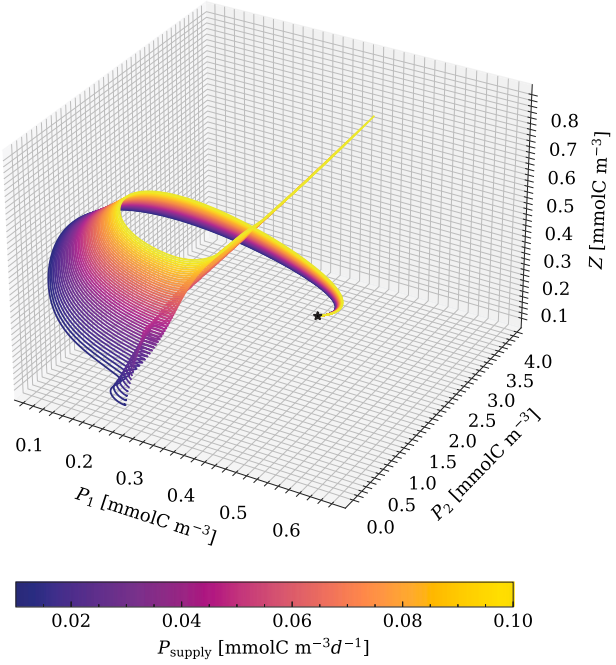

Fig. B.15. Trajectories of plankton biomass in a 3D phase space for a 2000-days simulation. The colour of each trajectory represents the parameter N_{supply} within the range of 50 values between 0.01 and 0.10. The black star represents the initial conditions, so this figure shows that, depending on N_{supply} , different equilibrium solutions are calculated.

by Mangolte et al. (2022) where increased phytoplankton biomass, following nutrient input, raises the common phytoplankton predator's biomass. During the dominance threshold time, P_1 is more grazed than P_2, favouring the latter and creating PCTs. Our results also showed a lack of competitive exclusion: both phytoplankton groups coexist for all three sets of simulations. Previous *in situ* observations showed that the front increases the biomass of several phytoplankton groups and not just diatoms (Mangolte et al., 2023). Our study reveals that even in a variable environment PCTs are influenced by the synergy of bottom-up and top-down controls which also act as a function of the number of pulses and their intensity.

4.3. A theoretical framework for fine-scale observations

Fig. 9 summarizes both *in situ* observations (top panel) and modelling results (bottom panel). The *in situ* R-ratio was computed from PROTEVSMED-SWOT cruise data by dividing the biomass of the smaller cytometric groups (PICO and NANO1, higher in the south of the front) by the total biomass at each sampled point. The scatter plot clearly depicts the shift from smaller phytoplankton dominance in the south to larger phytoplankton dominance in the north. The steepest gradient is located at latitude 38.5°N, identified as the position of the front (Tzortzis et al., 2021). In the south, there was fresher Atlantic water that recently entered the Mediterranean, while the north exhibited saltier surface water from the western Mediterranean circulation. This circulation is known to enrich the surface water in nutrients (Millot and Taupier-Letage, 2005). Despite the absence of nutrient measurements during the PROTEVSMED-SWOT cruise, our model, linking nutrient supply to the transition to larger phytoplankton, generally explains the observations well, except for the *in situ* total biomass which is lower in the north, contrary to observations. We attribute this discrepancy to limitations of the cytometry methodology, as flow cytometers are known to provide less accurate counts of large cells (Cunningham and Buonnacorsi, 1992; Peperzak et al., 2018). This leads to an underestimation of the abundance and size of the MICRO group, which makes a significant contribution to biomass. Satellite-derived chlorophyll surface concentration was higher in the north (Fig. 9, top panel), in agreement with the model results.

Despite its simplifications, the model allows us to better understand the mechanisms underlying the observations, as illustrated in Fig. 9 (bottom panel). In nutrient-poor waters (left side), P_1 dominates due to its higher growth rate at low nutrients concentrations. By increasing

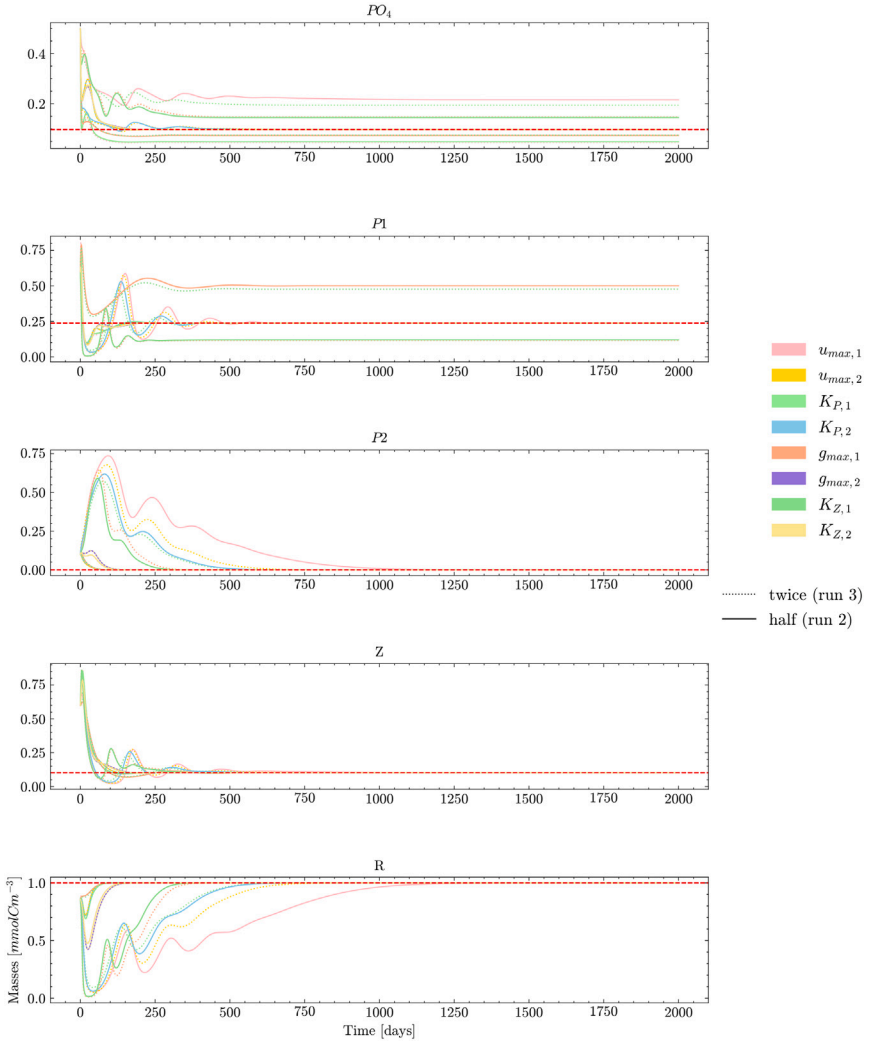

Fig. B.16. Sensitivity test with N_{supply} equal to 0.01 mmolC m^{-3} d^{-1}. The different colours of the curves represent the parameters tested. Solid curves represent execution with half the default value (run 2), and dashed curves represent execution with twice the default value (run 3). The dotted red line represents the default value.

N_{supply}, the model reaches a level allowing the emergence of P_2 , i.e. the coexistence threshold. Zooplankton then controls both phytoplankton groups, with a higher grazing pressure on P_1. Both phytoplankton groups thrive more at a higher value of N_{supply}, but P_1 is grazed more, leading to the dominance of P_2 beyond the dominance threshold. This result underlines that fronts have a significant role on PCTs, as the effect of grazing is significantly amplified by fine-scale dynamics (Rivière and Pondaven, 2006). Weak environmental gradients lead to dramatic shifts in phytoplankton communities, evident by the steep slope near the dominance threshold in (Fig. 9), making fronts regions of sharp phytoplankton distribution gradients (Taylor et al., 2012). Our results confirm the structuring effect of fine-scale fronts on the plankton community created by both pulsed nutrient supply and separated fluid dynamical niches (Lévy et al., 2018; d'Ovidio et al., 2010).

The proposed mechanism offers valuable insights into understanding PCTs, suggesting that diversity in oligotrophic regions is maintained by the patchy nature of the ocean. In oligotrophic environments, like the Mediterranean Sea, this patchiness allows different size classes of phytoplankton to thrive under varying conditions despite low nutrient availability. Even minor variations in nutrient fluxes can significantly influence phytoplankton community structure by varying the ratio between the different size classes. Shifting this ratio towards critical thresholds, such as dominance and coexistence thresholds, helps maintain biomass production and promote diversity. Previous work also highlighted the importance of these minor variations of nutrients. For instance, orthophosphate addition in the Cyprus Gyre (Eastern Mediterranean) shifted the microbial community composition towards larger organisms and the food web towards heterotrophic organisms (Flaten et al., 2005). Thingstad (2005) observed that phosphate limitation in the Mediterranean Sea is transmitted to higher trophic levels through a rapid predator response following phosphate addition. Findings of Flaten et al. (2005), Thingstad (2005) and Tzortzis et al. (2023) and this study suggest that, in response to nutrient addition potentially induced by fine-scale processes, the physiological state of primary producers and the plankton community composition change, which could lead to PCTs in oligotrophic regions. These fine-scale contrasts resemble large-scale contrasts, as biotic interactions across large-scale transition zones are also influenced by gradients in resource supply (Dutkiewicz et al., 2024).

4.4. Model caveats

Our study of PCTs intentionally relies on a strongly simplified model which overlooks key aspects of phytoplankton ecology required for realistic simulations. Our model does not account for phytoplankton's intrinsic dynamics such as photo-acclimation and variable stoichiometry, which improve agreement with observations, especially in oligotrophic conditions (Ayata, 2013). Our 0D model lacks spatial heterogeneity, missing important gradients and localized variations in environmental

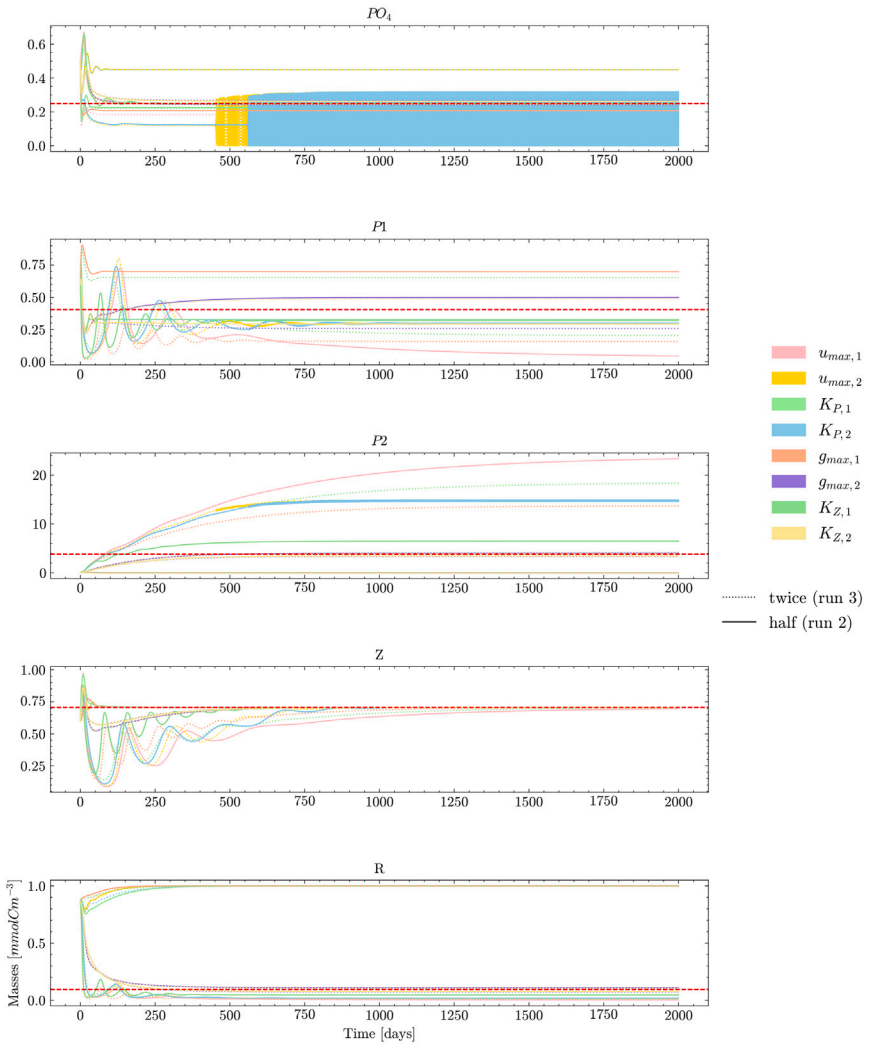

Fig. B.17. Sensitivity test with N_{supply} equal to 0.10 mmolC m^{-3} d^{-1}. The different colours of the curves represent the parameters tested. Solid curves represent execution with half the default value (run 2), and dashed curves represent execution with twice the default value (run 3). The dotted red line represents the default value.

factors such as light availability, nutrient concentrations, temperature, and mixing processes, which can lead to significant differences in phytoplankton growth rates and community composition (Mahadevan, 2005). An obvious limitation of our model is the restricted number of state variables instead of more complex modelling with multiple plankton groups and nutrient pools. Previous studies developed complex models incorporating the effects of temperature as well as the dynamics of the microbial loop (e.g. in the Mediterranean Sea, Auger et al., 2011; Aumont et al., 2015; Baklouti et al., 2021). Nevertheless, simple models are able to represent the global ecosystem features described by a complex model (Raick et al., 2006) with the advantage of being easier to interpret. Indeed, foundational principles are identical and qualitative behaviours are similar in both simple and complex models (e.g. Behrenfeld and Boss, 2014). Moreover, our results are consistent with results obtained from more complex models, including the fact that the composition of the community structure is explained by the synergy of bottom-up and top-down controls (e.g. Sailley et al., 2013). More recently, Mangolte et al. (2023), using an ecosystem model including multiple functional groups and sizes of plankton and coupling it with a circulation model, showed that the planktonic ecosystem response to enhanced nutrient supply at fronts is more complex than the pure bottom-up response because of ecological interactions such as shared predation, as we found with our simplified model.

Steady-state and pulsed forcing simulations also have their specific limitations. The advantage of the constant forcing analysis is that it allows for a clear understanding of the steady state model behaviour, which will facilitate its integration into a more complex framework, such as spatially- and temporally-resolved simulations. However, the model solutions (including in steady-state) strongly depend on the parameter values (see Fig. 7), and there are significant uncertainties regarding these parameters due to the challenges in obtaining accurate *in situ* measurements. The pulsed forcing analysis omits critical aspects of the complex coupling between physical processes and biological responses. For instance, the timing of phytoplankton growth is a crucial factor that varies with seasonal cycles, phytoplankton life cycles, flow dynamics, and nutrient availability. Simplifying these interactions with a step function assumes a temporally regular environment, whereas in the ocean, these processes are far less predictable and more irregular. As a result, the model does not fully capture the nuances of how physical variability influences biological dynamics in natural conditions, especially considering the mismatch between the scales of physical fronts and biological processes (Franks, 1992).

5. Concluding remarks and perspectives

Within a theoretical framework, we explored the phytoplankton community transitions (PCTs) observed during the PROTEVSMED-SWOT cruise. The question, "How do fine-scale dynamics explain PCTs?", is answered by fine-scale dynamics shaping the nutrient seascape and creating PCTs via cascading effects of nutrient transfer

through the plankton food chain. The phytoplankton uptake at different nutrient supply levels, combined with the grazing forcing, generates the coexistence and dominance thresholds. PCTs occur at the scale of water masses, where constant N_{supply} conditions lead to spatial PCTs, and also at the scale of fronts, where variable N_{supply} conditions lead to temporal PCTs. Comparison with *in situ* data validates the use of such a simple model to study PCTs in terms of qualitative behaviours. These results, derived from simple formulations, help us to understand the much more complex behaviour of phytoplankton cells adapted to fine-scale habitats. This work also informed the planning of the BioSWOT-Med cruise (Doglioli and Gregori, 2023), where high-resolution measurements of nutrient concentration and plankton diversity were taken across a front, along with a mesocosm experiment to measure zooplankton grazing. In future studies, this model will be spatialised and enhanced with high-resolution data from the BioSWOT-Med cruise, now benefiting from high-resolution SWOT data. The goal will be to study the fine-scale dynamics of plankton communities using a Lagrangian framework, adapting the growth-advection method (Messié et al., 2022) for oligotrophic areas like the Mediterranean Sea.

Funding

Laurina Oms' Ph.D. studentship is co-funded by the CNES (Centre National d'Etudes Spatiales), France and the Institute of Ocean Sciences (Aix-Marseille University). This research has been conducted in the framework of the project BioSWOT-AdAC (PIs F.d'Ovidio and A.Doglioli, https://www.swot-adac.org/, last access: 21 December 2023), funded by the TOSCA program of CNES. The MIO Axes Transverses program "AT-COUPLAGE" and the Sino-French IRP (CNR-CAS) DYF2M program also supported this work. The flow cytometer was funded by the CHROME project, Excellence Initiative of Aix-Marseille University – A*MIDEX, a French 11 Investissements d'Avenir program. The project leading to this publication received funding from the European FEDER Fund under project number 1166-39417.

CRediT authorship contribution statement

Laurina Oms: Writing – original draft, Visualization, Software, Methodology, Investigation, Formal analysis, Data curation, Conceptualization. **Monique Messié:** Writing – review & editing, Validation, Methodology, Investigation, Conceptualization. **Jean-Christophe Poggiale:** Writing – review & editing, Formal analysis. **Gérald Grégori:** Writing – review & editing, Validation, Supervision, Funding acquisition. **Andrea Doglioli:** Writing – review & editing, Validation, Supervision, Methodology, Investigation, Funding acquisition, Conceptualization.

Declaration of competing interest

The authors declare that they have no known competing financial interests or personal relationships that could have appeared to influence the work reported in this paper.

Acknowledgements

The authors thank Elvira Pulido-Villena for precious discussions about nutrient fluxes. Melilotus Thyssen is acknowledged for providing the CytoBuoy flow cytometer, Roxane Tzortzis and Lloyd Izard for the cytometry data analysis. The authors thank Franck Dumas and the crew of the RV Beautemps-Beaupré for shipboard operations.

Appendix A. PROTEVSMED-SWOT cruise

Fig. A.10 shows the data from the SeaSoar towed vehicle, which enabled (Tzortzis et al., 2021) to identify two surface water masses on either side of a zonal front, whose position is estimated at 38.5° N (cyan dots). The change in latitude clearly distinguishes the southern water mass (warmer and less salty) from the northern water mass (colder and saltier). Below the 28.5 isopycnal, intermediate waters are observed.

Appendix B. Model

B.1. Grazing experiments

We present here the results of different configurations for grazing pressure.

B.1.1. "No grazing"

When grazing rates are set to 0 in the complete model, no equilibria were identified. Fig. B.12 illustrates that in the absence of grazing, the P_1 biomass increases infinitely over time for N_{supply} values of 0.01 and 0.10 $\text{mmolC}\,\text{m}^{-3}\,\text{d}^{-1}$. The same figure highlights that coexistence is unattainable without grazing, evidenced by a constant R-ratio of 1 across the entire N_{supply} range.

B.1.2. "Equal grazing"

When grazing rates are set equal for P_1 and P_2 in the complete model, equilibria were identified. Fig. B.13 illustrates that in the presence of equal grazing, all masses reaches equilibrium over time for N_{supply} values of 0.01 and 0.10 $\text{mmolC}\,\text{m}^{-3}\,\text{d}^{-1}$. However, the same figure highlights that coexistence is unattainable with equal grazing, as evidenced by a constant R-ratio of 1 across the entire N_{supply} range.

B.1.3. "Differential grazing"

When Z is differentially set for P_1 and P_2 in the complete model (with a preference for P_1), equilibria were identified. Fig. B.15 illustrates in the phase space that in the presence of differential grazing, the system reaches equilibrium across the entire N_{supply} range, allowing for coexistence between P_1 and P_2 . The values of these equilibria vary based on the N_{supply} value. Fig. B.14 shows that, for 10 values of N_{supply} , the equilibrium state is reached for a 2000-days simulation time.

B.2. Sensitivity tests

The sensitivity analysis indicates that specific parameters exert notable effects on state variables, with a more pronounced effect observed when N_{supply} is set to 0.10 $\text{mmolC}, \text{m}^{-3}\,\text{d}^{-1}$. These results are associated with the interplay between nutrient availability, P_1 uptake, and P_2 uptake.

Fig. B.16 illustrates the temporal evolution of eight parameters across three runs, with N_{supply} set to 0.01 $\text{mmolC}, \text{m}^{-3}\,\text{d}^{-1}$. Notably, changes in parameter values primarily impact only N and P_1 among the state variables.

When $u_{max,1}$ is halved, it leads to a higher N value compared to its default and double values, resulting in a negative percentage of variation. Doubling $K_{P,1}$ results in a higher N value compared to its default and halved values, leading to a positive percentage of variation.

Halving $g_{max,1}$ results in a higher P_1 value and a negative percentage of variation. Simultaneously, this leads to a lower N value compared to its default and halved values, resulting in a positive percentage of variation.

Doubling $K_{Z,1}$ results in a higher P_1 value and a positive percentage of variation. Conversely, halving $K_{Z,1}$ leads to a higher N value compared to its default and double values, causing a negative percentage of variation.

Fig. B.17 depicts the temporal evolution of eight parameters across three runs, with N_{supply} set to 0.10 $\text{mmolC}, \text{m}^{-3}\,\text{d}^{-1}$. Notably, changes in parameter values significantly influence the state variables, particularly P_2 and the R-ratio.

When $u_{max,1}$ is halved, it leads to a higher P_2 value compared to its default and double values. This results in a negative percentage of variation and a positive R-ratio percentage of variation. Similarly, halving $u_{max,2}$ results in a higher N value compared to its default and double values, causing a negative percentage of variation. Conversely,

the percentage of variation of P_1 is negative, leading to a positive R-ratio percentage of variation.

Doubling $K_{P,1}$ leads to a higher P_2 value compared to its default and halved values, resulting in a positive percentage of variation and, consequently, a negative R-ratio percentage of variation. Conversely, halving $K_{P,2}$ results in a higher P_2 value compared to its default and double values, leading to a negative percentage of variation and, consequently, a positive R-ratio percentage of variation.

When $g_{max,1}$ is halved, it leads to a higher P_1 value and a negative percentage of variation. However, a lower P_2 value compared to its default and double values results in a positive percentage of variation and, consequently, a negative R-ratio percentage of variation.

Doubling $K_{Z,1}$ results in a higher P_1 value and a positive percentage of variation. Conversely, doubling $K_{Z,1}$ leads to a lower P_2 value compared to its default and halved values, causing a negative percentage of variation.

Data availability

The GitHub repository containing the data and code is available at: https://github.com/OmsLaurina/toolbox_growthmodel.

References

Acha, E.M., Piola, A., Iribarne, O., Mianzan, H., 2015. Ecological Processes at Marine Fronts: Oases in the Ocean. Springer.

Adjou, M., Bendtsen, J., Richardson, K., 2012. Modeling the influence from ocean transport, mixing and grazing on phytoplankton diversity. Ecol. Model. 225, 19–27. http://dx.doi.org/10.1016/j.ecolmodel.2011.11.005.

Auger, P.-A., Diaz, F., Ulses, C., Estournel, C., Neveux, J., Joux, F., Pujo-Pay, M., Naudin, J., 2011. Functioning of the planktonic ecosystem on the gulf of lions shelf (NW Mediterranean) during spring and its impact on the carbon deposition: a field data and 3-D modelling combined approach. Biogeosciences 8 (11), 3231–3261. http://dx.doi.org/10.5194/bg-8-3231-2011.

Aumont, O., Éthé, C., Tagliabue, A., Bopp, L., Gehlen, M., 2015. PISCES-v2: an ocean biogeochemical model for carbon and ecosystem studies. Geosci. Model Dev. Discuss. 8 (2), 1375–1509. http://dx.doi.org/10.5194/gmdd-8-1375-2015.

Ayata, S.-D., 2013. Phytoplankton growth formulation in marine ecosystem models: should we take into account photo-acclimation and variable stoichiometry in oligotrophic areas? J. Mar. Syst. 125, 29–40. http://dx.doi.org/10.1016/j.jmarsys.2012.12.010.

Baklouti, M., Pagès, R., Alekseenko, E., Guyennon, A., Grégori, G., 2021. On the benefits of using cell quotas in addition to intracellular elemental ratios in flexible-stoichiometry plankton functional type models. application to the mediterranean sea. Prog. Oceanogr. 197, 102634. http://dx.doi.org/10.1016/j.pocean.2021.102634.

Barton, A.D., Dutkiewicz, S., Flierl, G., Bragg, J., Follows, M.J., 2010. Patterns of diversity in marine phytoplankton. Science 327 (5972), 1509–1511.

Behrenfeld, M.J., Boss, E.S., 2014. Resurrecting the ecological underpinnings of ocean plankton blooms. Ann. Rev. Mar. Sci. 6, 167–194. http://dx.doi.org/10.1146/annurev-marine-052913-021325.

Bethoux, J., Gentili, B., Morin, P., Nicolas, E., Pierre, C., Ruiz-Pino, D., 1999. The mediterranean sea: a miniature ocean for climatic and environmental studies and a key for the climatic functioning of the North Atlantic. Prog. Oceanogr. 44 (1–3), 131–146. http://dx.doi.org/10.1016/S0079-6611(99)00023-3.

Bianchi, C.N., Morri, C., 2000. Marine biodiversity of the Mediterranean Sea: situation, problems and prospects for future research. Mar. Pollut. Bull. 40 (5), 367–376. http://dx.doi.org/10.1016/S0025-326X(00)00027-8.

Bohannan, B.J., Lenski, R.E., 2000. The relative importance of competition and predation varies with productivity in a model community. Amer. Nat. 156 (4), 329–340. http://dx.doi.org/10.1086/303393.

Clayton, S., Lin, Y.-C., Follows, M.J., Worden, A.Z., 2017. Co-existence of distinct ostreococcus ecotypes at an oceanic front. Limnol. Oceanogr. 62 (1), 75–88. http://dx.doi.org/10.1002/lno.10373.

Clayton, S., Nagai, T., Follows, M.J., 2014. Fine scale phytoplankton community structure across the Kuroshio front. J. Plankton Res. 36 (4), 1017–1030. http://dx.doi.org/10.1093/plankt/fbu020.

Cunningham, A., Buonnacorsi, G.A., 1992. Narrow-angle forward light scattering from individual algal cells: implications for size and shape discrimination in flow cytometry. J. Plankton Res. 14 (2), 223–234. http://dx.doi.org/10.1093/plankt/14.2.223.

Doglioli, 2015. OSCAHR cruise, RV Téthys II. http://dx.doi.org/10.17600/15008800.

Doglioli and Gregori, 2023. BioSWOT-Med cruise, RV L'Atalante. http://dx.doi.org/10.17600/18002392.

d'Ovidio, F., De Monte, S., Alvain, S., Dandonneau, Y., Lévy, M., 2010. Fluid dynamical niches of phytoplankton types. Proc. Natl. Acad. Sci. 107 (43), 18366–18370. http://dx.doi.org/10.1073/pnas.1004620107.

Droop, M.R., 1983. 25 years of algal growth kinetics a personal view. http://dx.doi.org/10.1515/botm.1983.26.3.99.

Dumas, F., 2018. Protevsmed_swot_2018_leg1 cruise, RV beautemps-beaupré. http://dx.doi.org/10.17183/protevsmed-swot-2018-leg1.

Dutkiewicz, S., Cermeno, P., Jahn, O., Follows, M.J., Hickman, A.E., Taniguchi, D.A., Ward, B.A., 2020. Dimensions of marine phytoplankton diversity. Biogeosciences 17 (3), 609–634. http://dx.doi.org/10.5194/bg-17-609-2020.

Dutkiewicz, S., Follett, C.L., Follows, M.J., Henderikx-Freitas, F., Ribalet, F., Gradoville, M.R., Coesel, S.N., Farnelid, H., Finkel, Z.V., Irwin, A.J., et al., 2024. Multiple biotic interactions establish phytoplankton community structure across environmental gradients. Limnol. Oceanogr. http://dx.doi.org/10.1002/lno.12555.

Edwards, A.M., 2001. Adding detritus to a nutrient–phytoplankton–zooplankton model: a dynamical-systems approach. J. Plankton Res. 23 (4), 389–413. http://dx.doi.org/10.1093/plankt/23.4.389.

Flaten, G.A.F., Skjoldal, E.F., Krom, M.D., Law, C.S., Mantoura, R.F.C., Pitta, P., Psarra, S., Tanaka, T., Tselepides, A., Woodward, E.M.S., et al., 2005. Studies of the microbial P-cycle during a Lagrangian phosphate-addition experiment in the Eastern Mediterranean. Deep Sea Res. II 52 (22–23), 2928–2943. http://dx.doi.org/10.1016/j.dsr2.2005.08.010.

Foladori, P., Quaranta, A., Ziglio, G., 2008. Use of silica microspheres having refractive index similar to bacteria for conversion of flow cytometric forward light scatter into biovolume. Water Res. 42 (14), 3757–3766. http://dx.doi.org/10.1016/j.watres.2008.06.026.

Franks, P.J., 1992. Phytoplankton blooms at fronts: patterns, scales, and physical forcing mechanisms. Rev. Aquat. Sci. 6 (2), 121–137.

Franks, P.J., 2002. NPZ models of plankton dynamics: their construction, coupling to physics, and application. J. Oceanogr. 58 (2), 379–387. http://dx.doi.org/10.1023/A:1015874028196.

Frederiksen, M., Edwards, M., Richardson, A.J., Halliday, N.C., Wanless, S., 2006. From plankton to top predators: bottom-up control of a marine food web across four trophic levels. J. Anim. Ecol. 75 (6), 1259–1268. http://dx.doi.org/10.1111/j.1365-2656.2006.01148.x.

Gangrade, S., Franks, P.J., 2023. Phytoplankton patches at oceanic fronts are linked to coastal upwelling pulses: Observations and implications in the California current system. J. Geophys. Res.: Oceans 128 (3), e2022JC019095. http://dx.doi.org/10.1029/2022JC019095.

Grant, S.R., 2014. Phosphorus Uptake Kinetics and Growth of Marine Osmotrophs (Ph.D. thesis). [Honolulu]:[University of Hawaii at Manoa],[August 2014].

Grover, J.P., 1990. Resource competition in a variable environment: phytoplankton growing according to Monod's model. Amer. Nat. 136 (6), 771–789. http://dx.doi.org/10.1086/285131.

Guieu and Desboeufs, 2017. PEACETIME cruise, RV pourquoi pas? http://dx.doi.org/10.17600/17000300.

Hernández-Carrasco, I., Alou-Font, E., Dumont, P.-A., Cabornero, A., Allen, J., Orfila, A., 2020. Lagrangian flow effects on phytoplankton abundance and composition along filament-like structures. Prog. Oceanogr. 189, 102469. http://dx.doi.org/10.1016/j.pocean.2020.102469.

Hitchcock, G.L., Mariano, A.J., Rossby, T., 1993. Mesoscale pigment fields in the gulf stream: Observations in a meander crest and trough. J. Geophys. Res.: Oceans 98 (C5), 8425–8445. http://dx.doi.org/10.1029/92JC02911.

Lévy, M., 2015. Exploration of the critical depth hypothesis with a simple NPZ model. ICES J. Mar. Sci. 72 (6), 1916–1925. http://dx.doi.org/10.1093/icesjms/fsv016.

Lévy, M., Ferrari, R., Franks, P.J., Martin, A.P., Rivière, P., 2012. Bringing physics to life at the submesoscale. Geophys. Res. Lett. 39 (14), http://dx.doi.org/10.1029/2012gl052756.

Lévy, M., Franks, P.J., Smith, K.S., 2018. The role of submesoscale currents in structuring marine ecosystems. Nat. Commun. 9 (1), 4758. http://dx.doi.org/10.1038/s41467-018-07059-3.

Lévy, M., Jahn, O., Dutkiewicz, S., Follows, M.J., d'Ovidio, F., 2015. The dynamical landscape of marine phytoplankton diversity. J. R. Soc. Interface 12 (111), 20150481. http://dx.doi.org/10.1098/rsif.2015.0481.

Lévy, M., Klein, P., Treguier, A.-M., 2001. Impact of sub-mesoscale physics on production and subduction of phytoplankton in an oligotrophic regime 59, 535–565. http://dx.doi.org/10.1357/002224001762842181.

Li, Q.P., Franks, P.J., Ohman, M.D., Landry, M.R., 2012. Enhanced nitrate fluxes and biological processes at a frontal zone in the southern California current system. J. Plankton Res. 34 (9), 790–801. http://dx.doi.org/10.1093/plankt/fbs006.

Longhurst, A., 1998. Ecological Geography of the Sea. Academic Press, San Diego, p. 398.

Mahadevan, A., 2005. Spatial heterogeneity and its relation to processes in the upper ocean. In: Ecosystem Function in Heterogeneous Landscapes. Springer, pp. 165–182.

Mahadevan, A., 2016. The impact of submesoscale physics on primary productivity of plankton. Ann. Rev. Mar. Sci. 8, 161–184. http://dx.doi.org/10.1146/annurev-marine-010814-015912.

Mahadevan, A., Archer, D., 2000. Modeling the impact of fronts and mesoscale circulation on the nutrient supply and biogeochemistry of the upper ocean. J. Geophys. Res.: Oceans 105 (C1), 1209–1225. http://dx.doi.org/10.1029/1999JC900216.

Mangolte, I., 2022. Effet Des Fronts Océaniques Sur Les Communautés De Plancton (Ph.D. thesis). Sorbonne Université.

Mangolte, I., Lévy, M., Dutkiewicz, S., Clayton, S., Jahn, O., 2022. Plankton community response to fronts: winners and losers. J. Plankton Res. 44 (2), 241–258. http://dx.doi.org/10.1093/plankt/fbac010.

Mangolte, I., Lévy, M., Haëck, C., Ohman, M.D., 2023. Sub-frontal niches of plankton communities driven by transport and trophic interactions at ocean fronts. http://dx.doi.org/10.5194/egusphere-2023-471.

Marra, J., Houghton, R., Garside, C., 1990. Phytoplankton growth at the shelf-break front in the Middle Atlantic bight.

Marrec, P., Grégori, G., Doglioli, A.M., Dugenne, M., Della Penna, A., Bhairy, N., Cariou, T., Hélias Nunige, S., Lahbib, S., Rougier, G., et al., 2018. Coupling physics and biogeochemistry thanks to high-resolution observations of the phytoplankton community structure in the northwestern mediterranean sea. Biogeosciences 15 (5), 1579–1606. http://dx.doi.org/10.5194/bg-15-1579-2018.

McCauley, E., Briand, F., 1979. Zooplankton grazing and phytoplankton species richness: Field tests of the predation hypothesis 1. Limnol. Oceanogr. 24 (2), 243–252. http://dx.doi.org/10.4319/lo.1979.24.2.0243.

McWilliams, J.C., 2021. Oceanic frontogenesis. Ann. Rev. Mar. Sci. 13, 227–253. http://dx.doi.org/10.1146/annurev-marine-032320-120725.

Menden-Deuer, S., Lessard, E.J., 2000. Carbon to volume relationships for dinoflagellates, diatoms, and other protist plankton. Limnol. Oceanogr. 45 (3), 569–579. http://dx.doi.org/10.4319/lo.2000.45.3.0569.

Messié, M., Chavez, F.P., 2017. Nutrient supply, surface currents, and plankton dynamics predict zooplankton hotspots in coastal upwelling systems. Geophys. Res. Lett. 44 (17), 8979–8986. http://dx.doi.org/10.1002/2017GL074322.

Messié, M., Sancho-Gallegos, D.A., Fiechter, J., Santora, J.A., Chavez, F.P., 2022. Satellite-based Lagrangian model reveals how upwelling and oceanic circulation shape krill hotspots in the California current system. Front. Mar. Sci. 9, 835813. http://dx.doi.org/10.3389/fmars.2022.835813.

Millot, C., Taupier-Letage, I., 2005. Circulation in the Mediterranean sea. Mediterranean Sea 29–66. http://dx.doi.org/10.1007/b107143.

Mitra, A., Flynn, K.J., Fasham, M.J., 2007. Accounting for grazing dynamics in nitrogen-phytoplankton-zooplankton (NPZ) models. Limnol. Oceanogr. 52 (2), 649–661. http://dx.doi.org/10.4319/lo.2007.52.2.0649.

Monod, J., 1942. Diauxie et respiration au cours de la croissance des cultures de b. coli. In: Annales de L'Institut Pasteur. Vol. 68, Elsevier, pp. 548–550.

Morán, X.A.G., LÓpez-urrutia, Á., Calvo-dÍaz, A., Li, W.K., 2010. Increasing importance of small phytoplankton in a warmer ocean. Global Change Biol. 16 (3), 1137–1144. http://dx.doi.org/10.1111/j.1365-2486.2009.01960.x.

Morrow, R., Fu, L.-L., Ardhuin, F., Benkiran, M., Chapron, B., Cosme, E., d'Ovidio, F., Farrar, J.T., Gille, S.T., Lapeyre, G., et al., 2019. Global observations of fine-scale ocean surface topography with the surface water and ocean topography (SWOT) mission. Front. Mar. Sci. 6, 232. http://dx.doi.org/10.3389/fmars.2019.00232.

Moutin, T., Doglioli, A.M., De Verneil, A., Bonnet, S., 2017. Preface: The oligotrophy to the ultra-oligotrophy pacific experiment (OUTPACE cruise, 18 february to 3 april 2015). Biogeosciences 14 (13), 3207–3220. http://dx.doi.org/10.5194/bg-14-3207-2017.

Moutin, T., Raimbault, P., 2002. Primary production, carbon export and nutrients availability in western and eastern mediterranean sea in early summer 1996 (MINOS cruise). J. Mar. Syst. 33, 273–288. http://dx.doi.org/10.1016/S0924-7963(02)00062-3.

Munkes, B., Löptien, U., Dietze, H., 2021. Cyanobacteria blooms in the baltic sea: a review of models and facts. Biogeosciences 18 (7), 2347–2378. http://dx.doi.org/10.5194/bg-18-2347-2021.

Peperzak, L., Zetsche, E.-M., Gollasch, S., Artigas, L.F., Bonato, S., Créach, V., Vré, P.d., Dubelaar, G.B., Henneghien, J., Hess-Erga, O.-K., et al., 2018. Comparing flow cytometry and microscopy in the quantification of vital aquatic organisms in ballast water. J. Mar. Eng. Technol. http://dx.doi.org/10.1080/20464177.2018.1525806.

Poggiale, J.-C., Baklouti, M., Queguiner, B., Kooijman, S., 2010. How far details are important in ecosystem modelling: the case of multi-limiting nutrients in phytoplankton–zooplankton interactions. Phil. Trans. R. Soc. B 365 (1557), 3495–3507. http://dx.doi.org/10.1098/rstb.2010.0165.

Poggiale, J.-C., Eynaud, Y., Baklouti, M., 2013. Impact of periodic nutrient input rate on trophic chain properties. Ecol. Complex. 14, 56–63. http://dx.doi.org/10.1016/j.ecocom.2013.01.005.

Polovina, J.J., Howell, E.A., Abecassis, M., 2008. Ocean's least productive waters are expanding. Geophys. Res. Lett. 35 (3), http://dx.doi.org/10.1029/2007GL031745.

Prowe, A.F., Pahlow, M., Dutkiewicz, S., Follows, M., Oschlies, A., 2012. Top-down control of marine phytoplankton diversity in a global ecosystem model. Prog. Oceanogr. 101 (1), 1–13. http://dx.doi.org/10.1016/j.pocean.2011.11.016.

Pulido-Villena, E., Desboeufs, K., Djaoudi, K., Van Wambeke, F., Barrillon, S., Doglioli, A., Petrenko, A., Taillandier, V., Fu, F., Gaillard, T., et al., 2021. Phosphorus cycling in the upper waters of the mediterranean sea (PEACETIME cruise): relative contribution of external and internal sources. Biogeosciences 18 (21), 5871–5889. http://dx.doi.org/10.5194/bg-18-5871-2021.

Raick, C., Soetaert, K., Grégoire, M., 2006. Model complexity and performance: how far can we simplify? Prog. Oceanogr. 70 (1), 27–57. http://dx.doi.org/10.1016/j.pocean.2006.03.001.

Rivière, P., Pondaven, P., 2006. Phytoplankton size classes competitions at sub-mesoscale in a frontal oceanic region. J. Mar. Syst. 60 (3–4), 345–364.

Sailley, S.F., Vogt, M., Doney, S.C., Aita, M.N., Bopp, L., Buitenhuis, E.T., Hashioka, T., Lima, I., Le Quéré, C., Yamanaka, Y., 2013. Comparing food web structures and dynamics across a suite of global marine ecosystem models. Ecol. Model. 261, 43–57. http://dx.doi.org/10.1016/j.ecolmodel.2013.04.006.

Siokou-Frangou, I., Christaki, U., Mazzocchi, M.G., Montresor, M., Ribera d'Alcalá, M., Vaqué, D., Zingone, A., 2010. Plankton in the open Mediterranean Sea: a review. Biogeosciences 7 (5), 1543–1586. http://dx.doi.org/10.5194/bg-7-1543-2010.

Taylor, A.G., Goericke, R., Landry, M.R., Selph, K.E., Wick, D.A., Roadman, M.J., 2012. Sharp gradients in phytoplankton community structure across a frontal zone in the California current ecosystem. J. Plankton Res. 34 (9), 778–789. http://dx.doi.org/10.1093/plankt/fbs036.

Thingstad, T., 2005. Simulating the response to phosphate additions in the oligotrophic eastern mediterranean using an idealized four-member microbial food web model. Deep Sea Res. II 52 (22–23), 3074–3089. http://dx.doi.org/10.1016/j.dsr2.2005.08.016.

Thingstad, T.F., Rassoulzadegan, F., 1999. Conceptual models for the biogeochemical role of the photic zone microbial food web, with particular reference to the Mediterranean Sea. Prog. Oceanogr. 44 (1–3), 271–286. http://dx.doi.org/10.1016/S0079-6611(99)00029-4.

Timmermans, K., Van der Wagt, B., Veldhuis, M., Maatman, A., De Baar, H., 2005. Physiological responses of three species of marine pico-phytoplankton to ammonium, phosphate, iron and light limitation. J. Sea Res. 53 (1–2), 109–120. http://dx.doi.org/10.1016/j.seares.2004.05.003.

Tzortzis, R., Doglioli, A.M., Barrillon, S., Petrenko, A.A., d'Ovidio, F., Izard, L., Thyssen, M., Pascual, A., Barceló-Llull, B., Cyr, F., et al., 2021. Impact of moderately energetic fine-scale dynamics on the phytoplankton community structure in the western Mediterranean Sea. Biogeosciences 18 (24), 6455–6477. http://dx.doi.org/10.5194/bg-18-6455-2021.

Tzortzis, R., Doglioli, A.M., Barrillon, S., Petrenko, A.A., Izard, L., Zhao, Y., d'Ovidio, F., Dumas, F., Gregori, G., 2023. The contrasted phytoplankton dynamics across a frontal system in the southwestern Mediterranean Sea. Biogeosciences 20 (16), 3491–3508. http://dx.doi.org/10.5194/bg-20-3491-2023.

Ward, B.A., Dutkiewicz, S., Follows, M.J., 2014. Modelling spatial and temporal patterns in size-structured marine plankton communities: top–down and bottom–up controls. J. Plankton Res. 36 (1), 31–47. http://dx.doi.org/10.1007/s00442-020-04768-9.

Yamamoto, T., Hatta, G., 2004. Pulsed nutrient supply as a factor inducing phytoplankton diversity. Ecol. Model. 171 (3), 247–270. http://dx.doi.org/10.1016/j.ecolmodel.2003.08.011.

Yoder, J.A., Ackleson, S.G., Barber, R.T., Flament, P., Balch, W.M., 1994. A line in the sea. Nature 371 (6499), 689–692.

Yoder, J.A., McClain, C.R., Blanton, J.O., Oeymay, L.-Y., 1987. Spatial scales in CZCS-chlorophyll imagery of the southeastern US continental shelf 1. Lao 32 (4), 929–941. http://dx.doi.org/10.4319/lo.1987.32.4.0929.

Zheng, Y., Gong, X., Gao, H., 2022. Selective grazing of zooplankton on phytoplankton defines rapid algal succession and blooms in oceans. Ecol. Model. 468, 109947. http://dx.doi.org/10.1016/j.ecolmodel.2022.109947.